https://doi.org/10.5194/egusphere-2026-2718
Preprint. Discussion started: 27 May 2026

Sediment characteristics regulate anaerobic oxidation of methane coupled with nitrate and nitrite in the hyporheic zone

Yujia Wang[1], Maja Bajic[2], Anja Wunderlich[1], Juergen Geist[3], William Orsi[2,4], Florian Einsiedl[1]

[1]Chair of Hydrogeology, School of Engineering and Design, Technical University of Munich, 80333 Munich, Germany
[2]Department of Earth and Environmental Sciences, Palaeontology & Geobiology, Ludwig-Maximilians-Universität München, 80333 Munich, Germany
[3]Chair of Aquatic Systems Biology, School of Life Sciences, Technical University of Munich, 80333 Munich, Germany
[4]GeoBio-CenterLMU, Ludwig-Maximilians-Universität München, 80333 Munich, Germany

Correspondence to: Florian Einsiedl (f.einsiedl@tum.de)

Abstract. Methane (CH_4) emissions from river systems contribute to the global greenhouse gas budget, but their contribution remains poorly constrained. Although proxies such as temperature, electron acceptor (EA) availability, and microbial communities are controlling factors, the role of the sediment characteristics (sediment permeability and organic carbon (OC) content) on anaerobic oxidation of methane (AOM) coupled with nitrate (NO_3^-)/nitrite (NO_2^-) is not well unterstood. Here, we investigated gravel-dominated, high-permeability sediments, where efficient advective transport promotes the deep penetration of terminal EAs such as oxygen (O_2), NO_3^- and sulfate (SO_4^{2-}) and inhibits microbial methane production. Conversely, hyporheic zone (HZ) sediment with fine-grained sediment was characterized by lower permeability, which restricts solute transport and facilitates diffusion-dominated processes and the development of anaerobic zones. Under these conditions, the presence of microbial available OC may support biological methane formation. Analyses of microbial communities of two profiles further indicate that also the distribution of methanogenic and methane-oxidizing taxa is closely linked to sediment permeability-controlled geochemical zonation. The 1D reactive transport modeling suggests that AOM with NO_3^- and NO_2^- as dominant EAs is selected for as a microbial process in the lower permeable sediments. Sediment permeability, therefore, regulated EA availability and, together with OC availability, shapes geochemical zonation, microbial community structure and the mechanism of AOM in the HZ. Therefore, sediment characteristics are shown here to strongly influence transport-reaction coupling, thereby regulating AOM and ultimately methane emissions from the HZ.

1 Introduction

Although freshwater ecosystems only cover a few percent of the Earth's terrestrial surface, they contribute significantly to the global methane budget, accounting for at least 25 % of global methane (CH_4) emissions, with lakes and rivers emitting about 159 Tg yr^{-1} during 2008-2017 (IPCC, 2021; Aben et al., 2017). Rivers exhibit particularly strong spatial and temporal heterogeneity in methane emissions, so considerable uncertainty can be assumed regarding their contribution to the global methane budget (Crawford et al., 2014b; Striegl et al., 2012). Consequently, enhancing our understanding of the mechanisms

https://doi.org/10.5194/egusphere-2026-2718
Preprint. Discussion started: 27 May 2026

and controls governing methane cycling in the hyporheic zone (HZ) of river systems is essential for accurately assessing and managing CH_4 emissions within the global carbon cycle.

In riverine systems, the HZ denotes the sedimentary domain located beneath and adjacent to the streambed, where active exchange occurs between surface water (SW) and groundwater (Sophocleous, 2002). The high diversity and metabolic activity of microbial communities within this zone favor intense biogeochemical reactions and drives the coexistence of multiple redox processes, thereby establishing the HZ as a crucial hotspot for methane cycling (Fischer et al., 2005; Hendricks, 1993). Once formed by methanogenesis in fine sediments, methane can be transported upward via two principal mechanisms: molecular diffusion and ebullition as gas bubbles (Baulch et al., 2011; Michaelis et al., 2024). These different transport processes can have fundamentally effects on microbial aerobic and anaerobic methane oxidation processes and emission rates from the HZ (Crawford et al., 2014a; Ma et al., 2022). Aerobic methane oxidation (MOx) is facilitated by aerobic methanotrophs, including members of the Gammaproteobacteria and related Alphaproteobacterial lineages, utilizing oxygen (O_2) as the terminal electron acceptor (EA) (Conrad, 2009; Buriánková et al., 2012). In contrast, anaerobic oxidation of methane (AOM) can be driven by various redox EAs such as nitrate (NO_3^-) and nitrite (NO_2^-) (Raghoebarsing et al., 2006; Ettwig et al., 2010). Nitrate-dependent anaerobic methane oxidation (NO_3^--DAMO) is controlled by ANME-2d archaea, specifically *Ca. Methanoperedens nitroreducens*, while nitrite-dependent anaerobic methane oxidation (NO_2^--DAMO) is mediated by bacteria of the genus *Ca. Methylomirabilis* within the NC10 phylum (Ettwig et al., 2010). Oswald et al. (2017) provided evidence that also *Crenothrix* spp. may transition from aerobic respiration to methane oxidation coupled with nitrate reduction under hypoxic conditions. The findings were also supported by further field studies that were performed in a dimictic lake and the HZ, where the microbial community patterns were linked to stable isotope measurements of methane (Einsiedl et al., 2020; Michaelis et al., 2022).

Previous studies have also shown that methane cycling in riverine HZs is influenced by interacting physical and biogeochemical drivers. Recent global syntheses further highlight temperature as a major driver of variability in denitrifying anaerobic methane oxidation across ecosystems (Jiang et al., 2026). Also exchange processes between SW and the HZ may influence methane dynamics by facilitating methane accumulation under conditions of poor water exchange, while enhanced exchange may improve the supply of oxidants and promotes methane oxidation (Sawakuchi et al., 2014; Michaelis et al., 2024). Furthermore, declining water levels and transient pressure perturbations can trigger episodic ebullition events from sedimentary gas reservoirs (Crawford et al., 2014a), while sediment characteristic such as dissolved organic carbon (DOC) content significantly influences methane production and oxidation, and consequently, emission dynamics in riverine HZs (Liu et al., 2020; Qin et al., 2020; Cui et al., 2025).

This study investigates methane oxidation coupled with nitrate/nitrite as a function of sediment grain size and permeability in the HZ using an integrated, multi-methodological approach. High-resolution porewater hydrochemical profiles from different sediment permeabilities were obtained by sediment peepers, while freeze-core sampling preserved sediment structure and facilitated depth-resolved microbial analyses. The abundance and diversity of microbial communities in

https://doi.org/10.5194/egusphere-2026-2718
Preprint. Discussion started: 27 May 2026

sediment columns of varying permeability were quantified using quantitative polymerase chain reaction (qPCR) and sequencing of 16S rRNA genes. Pore water profiles of dissolved oxygen and nitrate were linked with stable isotope profiles of dissolved methane and microbial distributions using two complementary modeling approaches. The one-dimensional inverse modeling software PROFILE (Berg et al., 1998)constrained depth-resolved net reaction zones of terminal EAs based on measured porewater profiles. Additionally, a process-based reactive transport model implemented in PHREEQC (Parkhurst and Appelo, 2013) explicitly evaluated methane oxidation pathways under transport-limited conditions. The results allowed an assessment of the relative importance of aerobic versus anaerobic methane oxidation with nitrate/nitrite when within HZ sediment columns of varying permeability.

https://doi.org/10.5194/egusphere-2026-2718
Preprint. Discussion started: 27 May 2026

2 Materials and Methods

2.1 Study site characterization

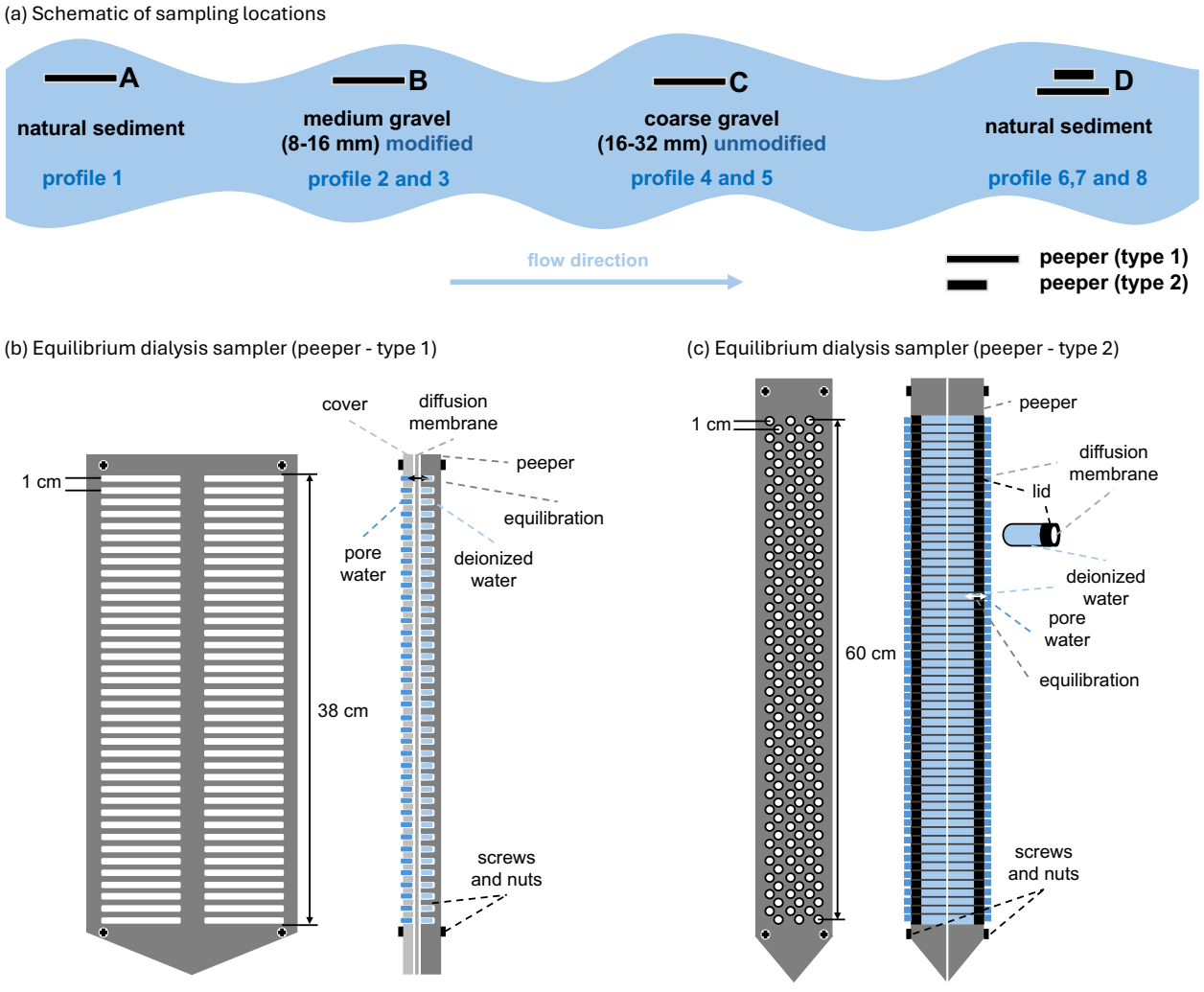

Figure 1: Schematic of the study area and porewater sampling devices. Schematic overview of the sampling design showing (a) the location of the investigated river reach and the positions of the sampling sites (A, B, C and D), together with the corresponding hydrochemical profiles obtained at each site, (b) the equilibrium dialysis sampler (peeper-type 1), and (c) the equilibrium dialysis sampler (peeper-type 2) employed in this study.

The catchment of the study stream, the Mühlangergraben, is composed of two significant geological units, the Tertiary hills and the Munich Gravel Plain (Pulg et al., 2013; Auerswald and Geist, 2017). The Mühlangergraben is an artificial lateral channel of the Moosach River, located in the southwest of Freising and approximately 30 kilometers northwest of Munich, Germany, and is diverted from the main River Moosach through a flap gate. After a flow-length of roughly 1.5 kilometers, Mühlangergraben merges with a small channel before rejoining the Moosach River system.

https://doi.org/10.5194/egusphere-2026-2718
Preprint. Discussion started: 27 May 2026

From September 2024 to September 2025, four different locations (A, B, C, and D) with a respective flow-distance of approximately 100 m were designated as experimental field-site (Fig. 1a). It is important to notice that in 2010, a riverbed gravel replenishment campaign was carried out at Mühlangergraben (locations B and C), while locations A and D show a natural and an unmodified river section. Two particle size gradations of gravel (8-16 mm (B) and 16-32 mm (C)) sourced from the same gravel quarry were used, creating a new gravel layer with a thickness between 20 and 40 cm. The pebbles primarily consist of well-rounded calcite. Beneath this new gravel layer, the original natural river sediment layer remained undisturbed. Here, it is worth mentioning that after one year of sediment exchange, although the particle size and dissolved oxygen levels remained higher than those recorded before the intervention, they were already approaching a state of partial re-clogging. This reduces hydraulic conductivity and diminishes contrasts attributable solely to gravel size (Pander et al., 2015), which is plausible given the relatively high sedimentation rates in stream systems in agriculturally dominated landscapes (Auerswald et al., 2019; Hoess and Geist, 2020).

Before the experiments started in 2024, sediment conditions at location B were deliberately altered within a 100 × 100 cm area to a depth of approximately 20 cm by removing fine particles from the pores while retaining the medium gravel (8-16 mm). Such stream bed lossenings are typical procedures used in stream bed restoration (Geist et al., 2023; Müller et al., 2014; Pander et al., 2015). In our experimental set-up, this modification aimed to differentiate location B from location C, where gravel replenishment had been succeeded by partial re-clogging resulting from fine-sediment infiltration. By establishing a gravel layer without fine sediments at one site, the study enabled the assessment of sediment-controlled effects on permeability, hydrochemical profile and geochemical gradients, and microbial processes under similar hydromorphological conditions.

2.2 Pore water sampling

Pore-water sampling was carried out between September 2024 and September 2025 at four locations (A-D) to characterize the hydrochemical profiles and geochemical gradients in the HZ (Fig. 1a). In situ equilibrium dialysis samplers (peepers) were installed to collect depth-resolved pore-water samples under minimally disturbed conditions. The study utilized two peeper designs: peeper-type 1 (Fig. 1b) applied at all sampling locations and peeper-type 2 with high-capacity (Fig. 1c), which was additionally deployed at location D (Fig. 1a). More details about the sampling are given in Sect. S1.

The first type of peeper adhered to the classical design outlined by Hesslein (1976). It featured a rigid body with two vertical columns, each containing 38 chambers at 1 cm resolution, yielding approximately 7 mL of pore water per depth interval. Each chamber was pre-filled with deionized water and sealed with a semi-permeable polyethersulfone membrane (pore size 0.2 µm; Cytiva Europe GmbH), secured by a Plexiglas cover and plastic screws (Michaelis et al., 2022). The second type of peeper consists of two modular plastic units that can be securely fastened together. Its design is based on a modified version of the bottle-insert peeper originally described by Teasdale (1995). Each pair of columns includes 60 glass vials spaced at 1

https://doi.org/10.5194/egusphere-2026-2718
Preprint. Discussion started: 27 May 2026

cm intervals, allowing a maximum sampling depth of 60 cm. Individual vials (1.5 mL) were filled with distilled water and sealed with PES membranes affixed to the vial caps. Following equilibration, the peeper provides up to 9 mL of pore water per depth interval (6 vials × 1.5 mL). Prior to sampling campaign, all vials were prepared, inserted into the peeper body, and the modules were assembled.

Peepers were manually inserted into the streambed, with most chambers embedded in the sediment and the uppermost chambers in contact with overlying water, aligned parallel to the flow direction to minimize disturbance. Equilibration between chamber water and surrounding pore water occurred via molecular diffusion across the semi-permeable membrane over at least three weeks, exceeding the commonly recommended period to ensure recovery of natural hydrochemical gradients after installation. Consequently, the collected samples represent time-averaged pore-water concentrations over the equilibration interval.

During the sampling, peepers were retrieved vertically from the streambed using a cable and pulley system, rinsed with deionized water, and processed immediately. Dissolved oxygen was measured in situ using a Clark-type microsensor (Unisense A/S, Aarhus, Denmark) within 10 minutes to minimize atmospheric contamination. Pore-water samples were extracted with sterile syringes. For methane concentration and $\delta^{13}C\text{-}CH_4$ analysis, ~3 mL of pore water was transferred into 10 mL glass vials pre-filled with 20 µL of 10 M NaOH and sealed with butyl rubber stoppers. Vials were flushed with synthetic air prior to sampling, and samples were injected with pressure equilibration to minimize degassing. Samples for ion analysis were collected in separate 1.5 mL vials pre-treated with 10 µL of 0.5 M NaOH (anions: Cl^-, NO_3^- , NO_2^-, SO_4^{2-}) or 10 µL of 1 M HNO_3 (NH_4^+). All samples were collected within 45 min, transported under cooled conditions, and stored refrigerated until analysis.

2.3 Water chemistry and stable isotope analysis

2.3.1 Anion and cation measurements

Dissolved anion and cation concentrations were quantified using ion chromatography with two independent Dionex ICS-1100 systems (Thermo Fisher Scientific, Dreieich, Germany). Anions were separated with a Dionex IonPac™ AS9-HC column, while cations were separated using a Dionex IonPac™ CS12A column. Calibration involved seven external concentration standards (Merck KGaA, Darmstadt, Germany). Each sample was analyzed in triplicate, and the reported concentrations represent the arithmetic mean of the three measurements. The analytical uncertainty was less than 10%. Detection limits (DLs) were established at 0.022 mmol L^{-1} for chloride (Cl^-), 0.013 mmol L^{-1} for NO_3^-, 0.003 mmol L^{-1} for NO_2^-, 0.008 mmol L^{-1} for sulfate (SO_4^{2-}), and 0.004 mmol L^{-1} for ammonium (NH_4^+).

https://doi.org/10.5194/egusphere-2026-2718
Preprint. Discussion started: 27 May 2026

2.3.2 CH_4 concentrations and $\delta^{13}C$ measurements of CH_4

Methane sampling and analytical procedures adhered to established equilibrium headspace techniques, representing methodological refinements of protocols recommended by the U.S. Environmental Protection Agency (EPA, 2001). Prior to gas chromatographic analysis, sample vials were equilibrated at room temperature for a minimum of 2 hours to ensure equilibrium between the dissolved and gaseous phases. Headspace methane concentrations were quantified using a TRACE 1300 gas chromatograph (Thermo Fisher Scientific, Dreieich, Germany) equipped with a TG-5MS capillary column and a flame ionization detector (FID). The instrument was calibrated with three certified methane standards (Rießner-Gase GmbH, Lichtenfels, Germany). For each vial, triplicate measurements were performed through manual injection of 250 µL of headspace gas. Total methane concentrations in the aqueous samples were calculated from the combined gas and water-phase methane contents using Henry's law, in accordance with the equilibrium headspace method described by Kampbell and Vandegrift (1998).

The same sample vials were subsequently utilized to determine the stable carbon isotopic ratio of methane ($\delta^{13}C$-CH_4). Isotope measurements were conducted using a cavity ring-down spectroscopy (CRDS) analyzer (G2201-i, Picarro Inc., Santa Clara, CA, USA) equipped with a Small Sample Introduction Module (SSIM) and calibrated against two reference gas standards (Airgas, Plumsteadville, PA, USA). Reliable isotope ratios were obtained only for headspace methane concentrations exceeding 30 ppm, and isotopic values were accepted only when at least two out of three replicate measurements surpassed the threshold concentration. Stable carbon isotope ratios are reported using conventional δ-notation relative to the Vienna Pee Dee Belemnite (VPDB) standard:

$$\delta^{13}\text{C-CH}_4 = \left(\frac{R_{sample}}{R_{standard}} - 1\right) \times 10^3 \quad (1)$$

where R_{sample} is the molar ratio of $^{13}C/^{12}C$ in the methane sample and $R_{standard}$ is the corresponding isotopic ratio of the VPDB reference standard.

2.4 Sediment sampling for grain-size, organic carbon content, and microbial community analyses

Sediment sampling was conducted in October 2024 at locations B and C using two approaches. Bulk sediment samples without depth resolution were collected on the day of pore-water sampling (17 October 2024) using a spade and plastic containers for grain-size analysis. This approach disturbs the natural sediment structure but provides an estimate of grain-size distribution. Grain-size composition was determined using sieve-slurry methods following DIN EN ISO 17892-4. Porosity, hydraulic conductivity, and sediment permeability were estimated based on the results derived from sieve analysis. More detailed procedures and results are given in Sect. S2.

Depth-resolved sediment samples were obtained on 29 October 2024 using the freeze-core method (Shapiro, 1958). At each location, two independent freeze cores were collected: one for microbial analyses and one for loss on ignition (LOI)

https://doi.org/10.5194/egusphere-2026-2718
Preprint. Discussion started: 27 May 2026

measurements. Liquid nitrogen was injected into the hyporheic zone via a hollow steel rod, freezing the surrounding sediment and allowing retrieval of largely undisturbed cores. Freeze cores for microbial analyses were sectioned at high vertical resolution. At location B, cores were sectioned from 0-31 cm (0-10 cm at 2 cm resolution, 10-31 cm at 3 cm resolution), and at location C from 0-36 cm (0-6 cm with a depth resolution of 2 cm, while the depth-solution from 6-36 cm was 3 cm). The fine sediment fraction from each interval was retained for microbial analyses. Separate freeze cores used for LOI measurements were sectioned at a coarser resolution of 10 cm, with total sampled depths of 30 cm at location B and 40 cm at location C. OC content was estimated as LOI following DIN EN 17685-1. Sediment samples were first dried at 110 ± 5 °C to constant mass. Coarse fractions (>2 mm) were separated, crushed, and homogenized with the fine fraction (<2 mm). Subsamples (4-5 g) were then combusted at 550 °C for 4 h, and LOI was calculated from mass loss relative to dry weight. The results at locations B and C are shown in Fig. S3.

2.5 Microbiological analysis

All sediment samples were promptly frozen following collection and stored at -22 °C until molecular analysis. For depth-resolved microbiological characterization, the sediment samples underwent DNA extraction, quantitative PCR (qPCR), and 16S rRNA gene amplicon sequencing.

For each depth interval, biological duplicates were processed independently. Total DNA was extracted from 0.5 g of sediment according to the protocol outlined by Vuillemin et al. (2019). The extracted DNA was diluted 1:10 with ultrapure PCR-grade water (Roche, Germany) before downstream applications, to remove PCR inhibitors. Quantification of prokaryotic 16S rRNA gene copy numbers was conducted using qPCR with the updated universal primer pair 515F (5′-GTG YCA GCM GCC GCG GTA A-3′) and 806R (5′-GGA CTA CNV GGG TWT CTA AT-3′), which enhances coverage of archaeal and marine lineages (Pichler et al., 2018).

All qPCR assays were conducted in 20 µL reaction volumes, which included 4 µL of diluted DNA template, SsoAdvanced Universal SYBR Green Supermix (Bio-Rad, Germany), primers (10 µM), MgCl2, and nuclease-free water. Amplifications were performed using a CFX Connect real-time PCR system (Bio-Rad). The thermal cycling protocol consisted of 40 cycles, beginning with denaturation at 95 °C for 15 s, followed by annealing and extension at 55 °C for 30 s. Standard curves were generated from gel-purified 16S rRNA gene amplicons, which were quantified using a Quant-iT dsDNA assay (Life Technologies, USA). An automated liquid handling system (epMotion 5070, Eppendorf) was employed to prepare dilution series ranging from 107 to 101 gene copies. All qPCR assays demonstrated amplification efficiencies between 90 % and 110 %, with coefficient of determination (R2) values exceeding 0.95.

For the analysis of microbial community composition, 16S rRNA gene amplicon libraries were generated using a consistent primer pair, each labeled with sample-specific barcodes as previously described (Pichler et al., 2018). PCR products were purified from 1.5 % agarose gels utilizing the QIAquick Gel Extraction Kit (Qiagen, Germany), quantified with a Qubit

https://doi.org/10.5194/egusphere-2026-2718
Preprint. Discussion started: 27 May 2026

dsDNA HS Assay Kit (Thermo Fisher Scientific), normalized to equimolar concentrations, and subsequently pooled. Library preparation adhered to the MiniSeq System Denature and Dilute Libraries Guide (Illumina), and sequencing was conducted on an Illumina MiniSeq platform at the GeoBio-CenterLMU.

Raw sequencing reads were processed as previously described (Michaelis et al., 2022) with USEARCH v10.0.240 for quality trimming, paired-end assembly, and operational taxonomic unit (OTU) clustering at 97 % sequence identity (Edgar, 2013). Representative OTU sequences were taxonomically assigned through BLASTn searches against the SILVA rRNA database (Quast et al., 2013). To identify and eliminate potential laboratory contaminants, extraction blanks and laboratory dust samples were sequenced concurrently and utilized to curate the OTU table according to established procedures (Pichler et al., 2018).

2.6 Inverse modeling of concentration gradients using PROFILE

To facilitate the interpretation of measured porewater profiles, the one-dimensional inverse modeling software PROFILE was utilized to identify the predominant redox reaction zones at various depths and to enable the quantitative inversion of the net redox reaction rates necessary to sustain the observed chemical concentration profiles (Berg et al., 1998). PROFILE operates within a steady-state mass conservation framework, which connects the concentration profile C(x) to an unknown net reaction term R(x) via the following Eq. (2):

$$\frac{d}{dx}\left[\varphi(D_s + D_b)\frac{dC}{dx}\right] + \varphi\,\alpha\big(C_0 - C(x)\big) + R(x) = 0 \qquad (2)$$

where x denotes sediment depth (cm), φ represents the sediment porosity (-), D_s is the effective molecular diffusion coefficient in sediments ($cm^2\ s^{-1}$), D_b signifies the bioturbation coefficient ($cm^2\ s^{-1}$), α indicates the irrigation coefficient (s^{-1}), and C_0 refers to the concentration at the sediment-water interface (µmol L^{-1}). In its general formulation, PROFILE accommodates molecular diffusion, bioturbation, and bio-irrigation as transport processes. PROFILE estimates the net reaction term R(x) by dividing the sediment profile into discrete depth intervals with constant reaction rates (µmol $L^{-1}\ s^{-1}$) and identifying the optimal zoning scheme that minimizes the sum of squared deviations between modeled and measured concentrations. The model's complexity is constrained through a built-in statistical F-test to prevent over-parameterization. Consequently, the resulting R(x) profiles represent net source-sink structures necessary to maintain the observed steady-state concentration gradients, rather than explicit rates of individual biogeochemical pathways.

As a first step, transport was considered purely diffusive, with bioturbation and bio-irrigation terms set to zero due to a lack of evidence for significant biological mixing or bio-irrigation. Measured porewater concentrations served as direct input for the model, with the sediment-water interface defined at a depth of 0 cm. Fixed concentration boundary conditions were applied at the upper boundary using values from the overlying water, while a zero-flux condition was implemented at the lower boundary. Additional details regarding parameterization are available in Sect. S3.

https://doi.org/10.5194/egusphere-2026-2718
Preprint. Discussion started: 27 May 2026

2.7 1D reactive transport model using PHREEQC

In addition, a one-dimensional reactive transport model was developed to account for hydraulic conditions within the HZ and to quantify the coupling between methane transport and microbially mediated redox transformations of terminal EAs. The model was implemented in PHREEQC using the TRANSPORT module with an operator-splitting approach, whereby solute transport and kinetic reactions are solved sequentially at each time step. Concentrations in PHREEQC are reported in mmol kg^{-1} water (mmol kg^{-1} w), which can be approximated as mmol L^{-1} for pore waters (assuming a water density close to 1 kg L^{-1}).

Solute transport of a dissolved species i was described by the one-dimensional advection-dispersion-reaction equation, Eq. (3):

$$\varphi \frac{\partial C_i}{\partial t} = \varphi D \frac{\partial^2 C_i}{\partial z^2} - \varphi v \frac{\partial C_i}{\partial z} + \varphi R_i \quad (3)$$

where C_i (mmol kg^{-1} w) denotes the aqueous concentration of species i, t (s) is time, and z (m) is the vertical coordinate. The porosity φ (-) represents the volumetric fraction of pore space available for solute transport and storage. The effective transport coefficient D (m^2 s^{-1}) represents the combined effects of molecular diffusion and mechanical dispersion, while v (m s^{-1}) denotes the advective velocity. The reaction term R_i (mmol kg^{-1} w s^{-1}) accounts for the net kinetic production or consumption rate within each grid cell. Constant concentration boundary conditions were prescribed at the upper and lower boundaries of the model domain, consistent with the PHREEQC transport formulation.

Methane oxidation was represented by three parallel Monod-type kinetic pathways, including aerobic methane oxidation (MOx) and anaerobic oxidation of methane (AOM). The aerobic pathway describes methane oxidation using oxygen as the terminal EA. The anaerobic pathways were formulated via two distinct mechanisms. In the first anaerobic pathway, nitrate reduction via heterotrophic denitrification produced nitrite, which was subsequently coupled to AOM and reduced to N_2. This formulation allows for a mass-consistent coupling between denitrification-derived nitrite production and NO_2^--DAMO, while maintaining aqueous NO_2^- concentrations near DL. In the second anaerobic pathway, methane oxidation was directly coupled to nitrate reduction, representing NO_3^--DAMO.

The rate formulation is derived from the Monod-based microbial growth kinetics proposed by Schäfer et al. (1998), but reformulated to quantify methane consumption rates under the assumption of a quasi-steady-state microbial biomass. For each pathway k, methane consumption was formulated as a dual-substrate Monod function reflecting co-limitation by methane and the corresponding terminal EA, Eq. (4):

$$r_k = \mu_{max,k} \frac{C_{CH_4}}{K_{S,CH_4,k} + C_{CH_4}} \frac{C_{EA,k}}{K_{S,EA,k} + C_{EA,k}} f_{a,k} X_k \frac{1}{Y_k}, \quad (4)$$

https://doi.org/10.5194/egusphere-2026-2718
Preprint. Discussion started: 27 May 2026

where r_k (mmol kg^{-1} w s^{-1}) denotes the methane consumption rate of pathway k, $\mu_{max,k}$ (s^{-1}) is an effective maximum kinetic rate constant, and X_k (g kg^{-1} w) is the microbial biomass associated with the respective pathway. C_{CH_4} and $C_{EA,k}$ (mmol kg^{-1} w) represent the concentrations of methane and the corresponding EA, while $K_{s,CH_4,k}$ and $K_{s,EA,k}$ (mmol kg^{-1} w) are half-saturation constants. The factor $f_{a,k}$ (-) denotes the active fraction of biomass. The yield coefficient Y_k (g biomass mmol^{-1} CH_4) links substrate consumption to biomass synthesis under idealized growth conditions and is used here as a stoichiometric scaling parameter converting biomass-specific metabolic potential into substrate consumption rates. Although microbial biomass is held constant during the simulation, methane oxidation is interpreted as being sustained by a dynamic balance between biomass production and biomass loss processes (including decay and dormancy), such that net changes in total biomass are negligible over the modeled timescale, aligning with the assumptions established by Monterroso et al., 2024). This assumption is further supported by physical constraints in porous sediments, where limited pore space and hydrodynamic shear restrict net biomass accumulation (Taylor and Jaffé, 1990). Microbial biomass X_k represents the total standing stock inferred from microbiological measurements and is prescribed as constant throughout the simulation. The activity factor $f_{a,k}$ is introduced to account for the fact that only a fraction of the total biomass is metabolically active at any given time; thus, the product $f_{a,k}\,X_k$ represents the effective active biomass participating in methane oxidation. Under this formulation, the Monod term describes effective methane consumption kinetics rather than explicit biomass dynamics.

In natural sedimentary environments, terminal EAs are consumed by multiple concurrent biogeochemical pathways, many of which are not explicitly resolved by available observations. To account for these unresolved processes while maintaining a parsimonious kinetic framework, EA consumption was partitioned into methane-coupled reactions and a background consumption term, the latter representing all non-methane-related electron-acceptor-consuming processes affecting both oxygen and nitrate. The background sink was formulated as a first-order decay process acting on the aqueous concentration of the respective EA Eq. (5):

$$r_{EA,BG} = -k_{EA,BG}\,C_{EA}, \tag{5}$$

where $r_{EA,BG}$ (mmol kg^{-1} w s^{-1}) denotes the background consumption rate of the EA, $k_{EA,BG}$ (s^{-1}) is a first-order rate constant, and C_{EA} (mmol kg^{-1} w) is the EA concentration.

The total reaction-driven methane consumption rate was calculated as the sum of all modeled methane oxidation pathways Eq. (6):

$$r_{CH_4,tot} = r_{MOx} + r_{NO_3^-\text{-DAMO}} + r_{NO_2^-\text{-DAMO}}, \tag{6}$$

where all rates are in mmol kg^{-1} w s^{-1}. More details on model setup and input parameters are provided in Sect. S4.

https://doi.org/10.5194/egusphere-2026-2718
Preprint. Discussion started: 27 May 2026

3 Results and discussion

3.1 High-resolution vertical hydrochemical profiles from the hyporheic zone

Figure 2 shows the eight vertical pore-water profiles obtained during the sampling campaign from October 2024 to September 2025. The profiles display depth-resolved solute concentrations, including dissolved oxygen, nitrate, nitrite, sulfate, as well as ammonium, chloride, methane, and $\delta^{13}C\text{-}CH_4$ values. The total depth of these profiles varies between 26 and 40 cm depending on the installation depth of the peeper which was limited due to the characteristic of the coarser sediment. The vertical HZ hydrochemical profiles from the coarser grained sediment with higher permeability (profiles 1-3 and 6-8) are characterized by the absence of methane and indicate non-methanogenic conditions within the sampling depth. In contrast, vertical HZ hydrochemical profiles from finer grained sediment with lower permeability (profiles 4 and 5) exhibit significant methane concentrations, thereby delineating a distinct methanogenic regime (Fig. 2a4-b4 and a5-b5).

Locations A (profile 1) and D (profiles 6, 7, and 8) represent natural gravel-dominated riverbeds, where gravels and stones prevail. Under these conditions, increased permeability is expected to result in enhanced exchange between SW and the HZ, and the OC at both locations is assumed to be relatively aged and potentially less reactive due to long-term undisturbed conditions, compared to location C (profiles 4 and 5). In contrast, finer grained sediments and reduced permeability at location C appear to result in strongly reducing redox conditions, thereby favoring methanogenesis (Fig. 2a4-b4 and a5-b5). At location B (profiles 2 and 3), fine sediments in the upper layer have been removed, further enhancing hydraulic permeability. These conditions likely promote strong hydrological exchange and oxidizing environments, preventing the development of sufficiently reducing conditions for methanogenesis. Although the limited amount of fine sediments at location B would result in lower OC content compared to location C, LOI results (Fig. S3) indicate broadly similar values at both locations. This apparent similarity may reflect the dominance of low OC at both sites. Besides the higher hydraulic permeability at location B compared to location C, its lower OC content may represent an additional constraint on methanogenesis.

https://doi.org/10.5194/egusphere-2026-2718
Preprint. Discussion started: 27 May 2026

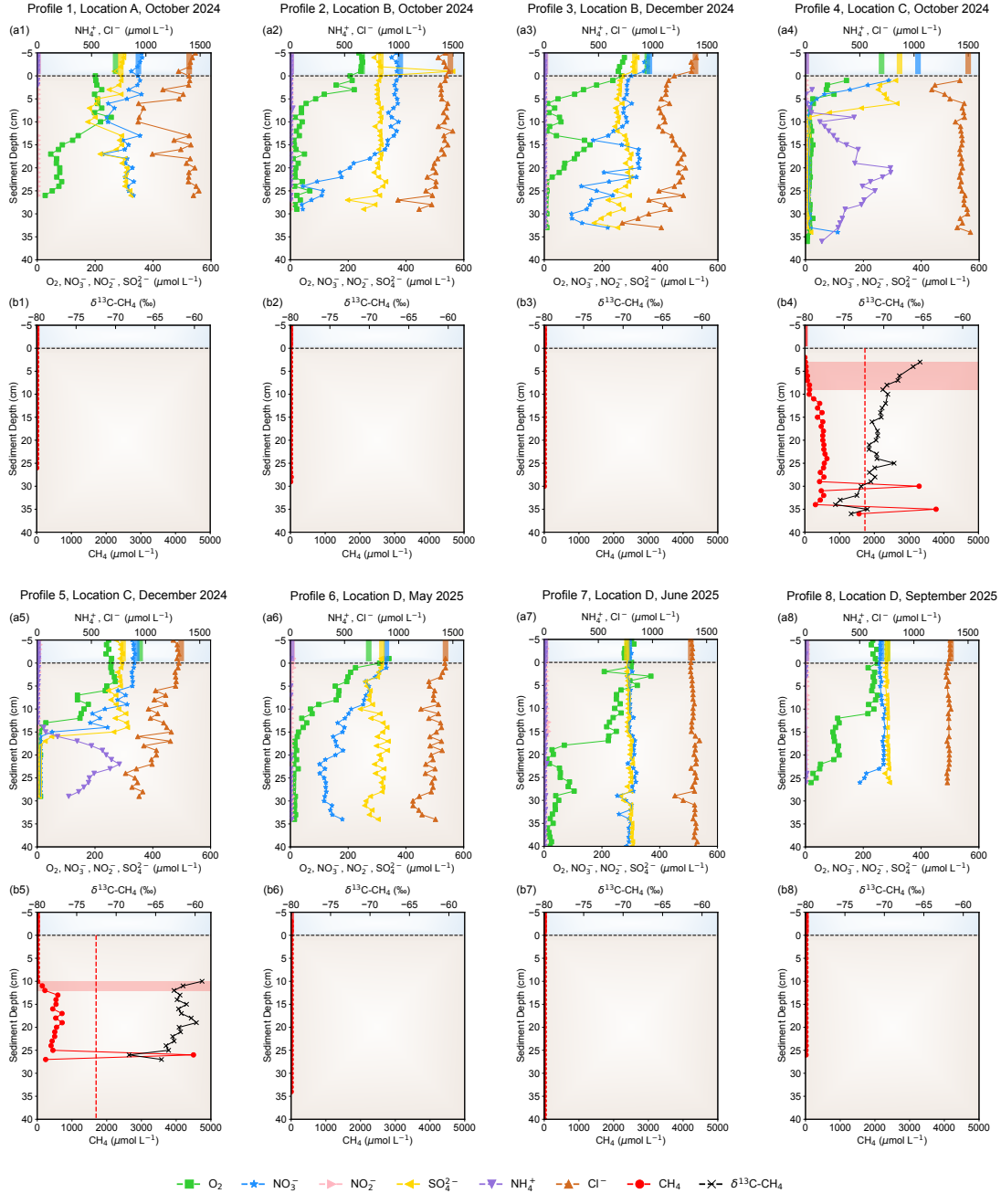

Figure 2. Depth-resolved porewater hydrochemical profiles across four sampling sites. Panels (a1) - (a8) display depth-resolved concentration profiles of O_2, NO_3^-, NO_2^-, SO_4^{2-}, Cl^- and NH_4^+. Panels (b1) - (b8) show CH_4 concentration together with $\delta^{13}C\text{-}CH_4$. Each pore-water profile is represented by a pair of panels (e.g., a1 and b1), which together display the high-resolution concentrations of solutes (x-axis) plotted against sediment depth (y-axis). Vertical bars above the interface represent solute concentrations in the overlying stream water. The horizontal black dashed line indicates the interface between the SW and the sediment. In panels (b4) and (b5), the red dashed line indicates the methane saturation concentration at in situ temperature, while the red shaded area denotes the zone of biological methane oxidation.

https://doi.org/10.5194/egusphere-2026-2718
Preprint. Discussion started: 27 May 2026

The vertical distribution patterns of terminal EAs, including dissolved oxygen, nitrate, and sulfate, reveal two distinct regimes across the profiles, reflecting different balances between solute transport and biogeochemical consumption in the HZ. The non-methanogenic patterns (profiles 1-3 and 6-8) are characterized by deep oxygen penetration, with O_2 concentrations gradually declining over the upper 25-30 cm of the sediment but remaining above 20-30 µmol L^{-1} throughout most of the profile. This results in predominantly oxic to micro-oxic conditions, where nitrate concentrations remain relatively constant with depth and decrease within the micro-oxic zone. Exactly there, several profiles (profiles 2,3,6 and 8) showing depth-dependent nitrate gradients that are not reflected in the conservative tracer Cl^-, which may result from the combined effects of redox zonation and microbial consumption. We assume heterotrophic nitrate reduction within the micro-oxic zone, in which OC may serve as the electron donor and as previously documented in other hyporheic environments (e.g. Hinkle et al., 2001). In contrast, profiles 1 and 7 maintain persistently oxic conditions, which may inhibit nitrate reduction throughout most of the sediment column. In profile 1, this inhibition is further reflected by nitrate fluctuations that closely track the conservative tracer Cl^-, indicating additional control by physical mixing processes and dilution (McMahon and Böhlke, 1996). Under these conditions, sulfate remains largely conservative throughout the monitored HZ, and there is no geochemical evidence of bacterial sulfate reduction from the pore water profiles at profile 1 suggests that strongly reducing conditions were not established here.

Subsurface methanogenic conditions were observed for deeper sediments in profiles 4 and 5 and exhibit, as expected, limited O_2 penetration, where oxygen depletion has occurred within the upper few centimeters of the HZ. These profiles are characterized by near-complete NO_3^- depletion below approximately 15 cm, which may indicate effective denitrification. Below that depth, bacterial sulfate reduction may have occurred following the depletion of NO_3^-. Compared to profile 4, sulfate reduction in profile 5 is shifted further downward and proceeds more gradually, consistent with delayed oxygen and nitrate reduction. This vertical displacement likely reflects kinetically constrained redox reactions under winter conditions (Herzog et al., 2025), resulting in strongly reducing environments being established only in deeper parts of the HZ. Overall, the depletion of nitrate and sulfate indicates the development of more reducing conditions compared to those observed in the non-methanogenic pattern.

Although denitrification may have occurred, NO_2^- concentrations generally remain close to the DL (3.05 µmol L^{-1}) across most profiles and depths, which may suggest that NO_2^- as a transient intermediate is still used microbiologically under anoxic conditions (e.g. Hassan et al., 2016).

Ammonium concentrations are generally low, remaining close to or below the analytical DL (3.89 µmol L^{-1}) throughout most of the sediment column. In contrast, profiles 4 and 5 display a markedly different pattern, characterized by consistently elevated NH_4^+ concentrations well above the DL. This increase is associated with more reducing redox conditions and may reflect organic matter mineralization under methanogenic conditions. Such an interpretation is consistent with previous findings from lake sediments, where microbial methane production was linked to an increase in NH_4^+ in the overlying water column (Einsiedl et al., 2020).

https://doi.org/10.5194/egusphere-2026-2718
Preprint. Discussion started: 27 May 2026

In profile 4, methane concentrations and $\delta^{13}C\text{-}CH_4$ values display distinct depth-dependent patterns that delineate specific zones of methane production, transport, and microbial oxidation. Below a depth of 24 cm, methane concentrations increase in a non-monotonic fashion, reaching exceptionally high levels at 30 and 35 cm (3290.64 and 3778.43 µmol L^{-1}), which significantly surpass the calculated in situ methane solubility of 1731.17 µmol L^{-1}. This marked supersaturation suggests the presence of a free gas phase and methane bubble formation within the sediment. The $\delta^{13}C\text{-}CH_4$ values in this deeper interval are notably depleted, with a mean of -72.45 ‰, which aligns with hydrogenotrophic and methylotrophic methanogenesis under anoxic conditions (Liu et al., 2013; Penger et al., 2012). Between depths of 9 and 24 cm, methane concentrations decrease monotonically toward the sediment surface, while $\delta^{13}C\text{-}CH_4$ values exhibit only minor isotopic enrichment (less than 1 ‰). This little isotopic shift suggests that methane attenuation within this interval is primarily governed by diffusion-controlled transport rather than significant biological oxidation. In contrast, a distinct methane regime is observed at depths of 0-9 cm. Methane concentrations decrease sharply toward the sediment-water interface, accompanied by isotopic enrichment in $\delta^{13}C\text{-}CH_4$ from -70.2 ‰ to -65.4 ‰. This shift indicates active microbially mediated methane oxidation in shallow sediments and is consistent with observations from other field studies (Michaelis et al., 2022; Thottathil et al., 2022). Profile 5 exhibits a broadly similar vertical distribution. However, all major reaction zones are shifted to greater depths compared to profile 4. This pattern may be consistent with a downward shift in the methane oxidation zone during winter conditions, likely driven by reduced microbial activity in the shallow sediment. These findings also match observations from other stream systems where the lowest redox conditions in sediment typically occur during summer, where the greatest difference in redox are found directly at the stream bed surface (Geist and Auerswald, 2007).

In summary, non-methanogenic profiles were observed at locations A, B, and D, whereas biological methanogenesis is occurring in the deeper sediment layers at location C. Although repeatedly sampled, locations B, C, and D reveal temporal variability in concentrations and in the shape of the gradients but show no fundamental alteration in the underlying biogeochemical mechanisms, including EA penetration, redox zonation, and the occurrence of methanogenesis. Instead, spatial heterogeneity, primarily through variations in sediment permeability and OC availability, may exert a stronger control on the biogeochemical processes compared to temporal variability. This spatial heterogeneity is driven by the differences in sediment characteristics (Sect. 2.1 and S2) and appears to be a dominant factor controlling reaction-transport coupling within the HZ.

https://doi.org/10.5194/egusphere-2026-2718
Preprint. Discussion started: 27 May 2026

3.2 Sediment characteristics determine chemical gradients as well as microbial community distribution

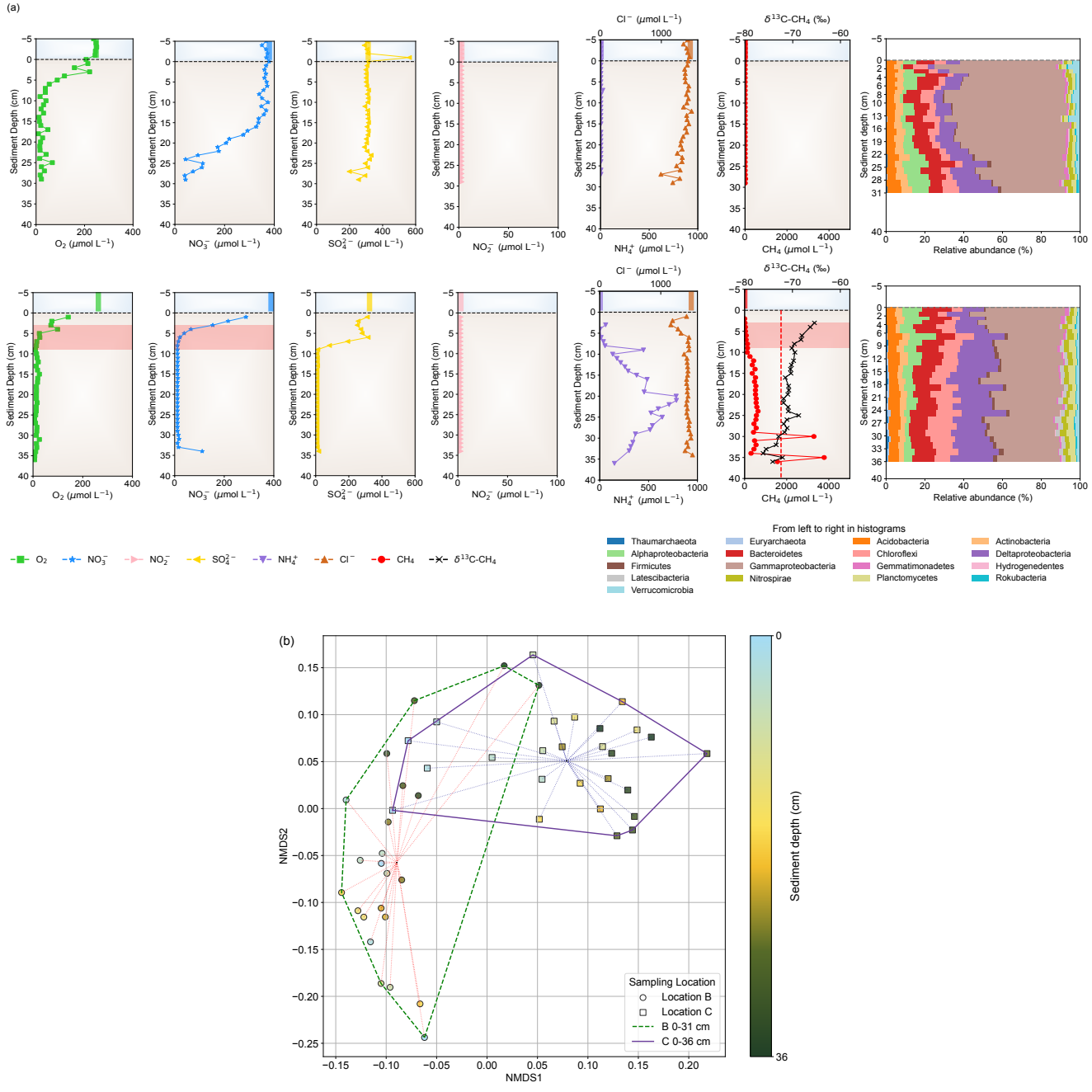

Figure 3. Comparison of porewater hydrochemistry and microbial community structure between locations B and C. (a) Depth-resolved hydrochemical profiles together with relative abundances of major microbial taxa at locations B and C. (b) Non-metric multidimensional scaling (NMDS) ordination of microbial community composition, illustrating differences in community dispersion between locations B and C.

https://doi.org/10.5194/egusphere-2026-2718
Preprint. Discussion started: 27 May 2026

Following the identification of two recurring pore-water regimes across the 8 profiles (non-methanogenic and methanogenic) we proceeded to examine two representative profiles (profiles 2 and 4) in greater detail. Specifically, we investigate how differences in sediment characteristics are associated with variations in EA penetration, redox zonation, and the microbial community distribution within the HZ. These profiles were chosen for their distinct sediment conditions, which minimize confounding effects related to sampling time and gravel-size heterogeneity. Additionally, their nitrate profiles exemplify two canonical geometries of terminal EA depth distribution (Jørgensen et al., 2024). Profile 2 displays a concave-up geometry, consistent with deeper EA penetration and sustained oxidant availability at depth. In contrast, profile 4 exhibits a concave-down pattern, indicative of rapid shallow depletion and the formation of an underlying anoxic zone.

At Location B, the upper sediment layer is composed of medium-sized gravel, from which fine material was experimentally removed before sampling. This process resulted in a highly permeable matrix characterized by well-connected pore spaces and limited OC availability. Beneath this layer, the sediment consists of an aged gravel layer that has experienced considerable fine-sediment infilling, resulting in partial pore clogging.

This structural contrast is clearly evident in pore-water chemistry of profile 2 (Fig. 3a). Dissolved oxygen decreases rapidly with depth, becoming largely depleted within the upper 9 cm. This trend indicates that oxygen consumption surpasses vertical resupply, resulting in a sharp oxic-suboxic transition even under advective conditions. Below this depth, oxygen levels remain low throughout the profile. Nitrate exhibits a response at the sediment modification boundary. In the modified gravel layer, nitrate concentrations closely resemble surface-water values, showing only minor attenuation despite oxygen depletion. This observation suggests that advective replenishment effectively balances the biological consumption. Below the modified layer, nitrate displays a pronounced concave-upward decline with depth, which coincides with reduced effective porosity due to fine-sediment infilling. This infilling may limit solute resupply and allows denitrification. Sulfate remains conservative throughout the profile, while nitrite, ammonium, and methane concentrations remain, as expected, below DLs. This pattern indicates that sustained nitrate availability may inhibit the development of strongly reducing conditions, thereby preventing bacterial sulfate reduction and methanogenesis.

Microbial community composition provides additional support for the transport-reaction mechanisms inferred from hydrochemical profiles (Fig. 3a). Across the sampled interval, communities are dominated by bacterial groups associated with aerobic and facultatively anaerobic heterotrophy, with Gammaproteobacteria and Alphaproteobacteria as the main taxa. This community structure is consistent with geochemical conditions characterized by rapid oxygen depletion in shallow sediments and sustained nitrate availability, favoring metabolically flexible taxa capable of switching between O_2 and NO_3^- as terminal EAs. Vertically, microbial communities exhibit depth-dependent variations corresponding to sediment stratification and redox zonation. Gammaproteobacteria dominate in shallow sediments with elevated oxygen fluxes, whereas Alphaproteobacteria increase below approximately 9 cm within the nitrate-reducing zone. Their coexistence across the oxic-suboxic transition suggests that the shift from aerobic respiration to denitrification may be primarily mediated by metabolic switching of facultatively anaerobic taxa (denitrifiers). Below the sediment modification zone, enhanced net

https://doi.org/10.5194/egusphere-2026-2718
Preprint. Discussion started: 27 May 2026

nitrate consumption coincides with reduced porosity, limited solute resupply, and a further increase in Alphaproteobacteria, indicating functional reorganization consistent with denitrification. Notably, no enrichment of methanogenic taxa is observed at any depth, in agreement with the absence of methane accumulation.

At location C, the sediment characteristics indicate significant partial re-sedimentation within the gravel framework. Grain-size composition is dominated by coarse gravel, with fine (sand- and clay-sized) fractions comprising approximately 15% of the total. This infilling markedly decreases effective porosity and hydraulic permeability, thereby limiting solute transport within the HZ and simultaneously enhancing OC availability through the retention of fine material.

This sediment texture and related permeability exert a strong influence on the pore-water chemical profile, resulting in a distinctly different pattern (profile 4) compared to profile 2. Restricted permeability significantly constrains the downward transport of EAs, resulting in porewater exchange that is predominantly governed by diffusion. Consequently, dissolved oxygen, nitrate, and sulfate are rapidly depleted within the shallow sediment. In the upper 0-7 cm, both oxygen and nitrate exhibit concurrent declines characterized by concave-down profiles, suggesting that biological consumption substantially surpasses vertical resupply. Within this interval, multiple EAs are utilized simultaneously, complicating the clear identification of the classical redox sequence based solely on hydrochemical profiles. At greater depths, sulfate reduction becomes distinctly evident, as sulfate concentrations decrease sharply within a narrow range of approximately 7-9 cm, signaling the initiation of sulfate-reducing conditions. Below this depth, the sustained limitation of EA supply fosters stable anaerobic conditions. Methane cycling exhibits a clear depth-dependent organization within this geochemical context, with methane concentrations and $\delta^{13}C\text{-}CH_4$ delineating a distinct three-zone structure. Below 24 cm, methane concentrations are elevated and locally surpass in situ solubility, suggesting gas-phase contact. Concurrently, strongly depleted $\delta^{13}C\text{-}CH_4$ values are indicative of hydrogenotrophic and methylotrophic methanogenesis (Liu et al., 2013; Penger et al., 2012). Correspondingly, NH_4^+ concentrations increase within this interval, likely reflecting enhanced organic matter mineralization during the methanogenic process. Between 9 and 24 cm, methane concentrations exhibit a monotonic decline accompanied by only minor isotopic enrichment, which aligns with diffusion-controlled upward transport. In the shallow sediment layer (0-9 cm), methane concentrations decrease sharply, while $\delta^{13}C\text{-}CH_4$ values demonstrate significant isotopic enrichment, thereby providing clear evidence of active microbial methane oxidation (Schubert et al., 2011).

Microbial community composition provides independent biological support for the redox zonation inferred from porewater geochemistry. Throughout the profiles at location C, microbial communities show minimal vertical variability and are dominated by metabolically flexible heterotrophic bacteria, with Gammaproteobacteria and Alphaproteobacteria consistently exhibiting the highest relative abundances. This composition suggests adaptation to organic matter degradation under fluctuating redox conditions. Euryarchaeota occur at low but stable abundances throughout the profile, indicating the presence of methanogenic lineages. Vertically, the shallow sediment interval (0-7 cm) exhibits relatively high and stable abundances of both Gammaproteobacteria and Alphaproteobacteria, which correspond to the concurrent depletion of dissolved oxygen and nitrate. This pattern may suggest the presence of anaerobic microenvironments within an overall oxic

https://doi.org/10.5194/egusphere-2026-2718
Preprint. Discussion started: 27 May 2026

zone and supports the co-occurrence of aerobic respiration and heterotrophic denitrification. In the sulfate-depletion zone (7-9 cm), taxa associated with sulfate reduction show a slight increase in relative abundance (Fig. 5), indicating a localized microbial response to sulfate-reducing conditions. Below 9 cm, community composition remains largely uniform at the phylum/class level, despite additional functional zonation indicated by NH_4^+ dynamics around 21 cm. At depths below 24 cm, Euryarchaeota increase progressively and coincide with elevated methane concentrations and strongly depleted $\delta^{13}C$-CH_4 values, suggesting that methanogenesis is driven by a numerically minor but highly specialized microbial community within the Euryarchaeota.

High-resolution microbial community abundance data provide complementary biological evidence for porewater geochemical patterns, while NMDS ordination offers an integrated, structure-based perspective on the influence of sediment characteristic on microbial spatial organization (Fig. 3b). At location B, sustained EA supply, combined with advection-dominated transport, fosters the development of pronounced redox zonation. Under these conditions, microbial community composition exhibits notable depth-dependent variation. The broad dispersion of samples in NMDS space indicates strong hydraulic exchange, which exposes microbial assemblages to a diverse array of dynamically evolving geochemical niches. In contrast, at location C, fine-sediment infilling leads to diffusion-dominated transport, which restricts the resupply of EAs and compresses redox zonation, resulting in the overlap of multiple reaction zones within a narrow depth interval. Consequently, microbial communities exhibit limited vertical differentiation regarding sulfate reduction and methanogenesis, while NMDS ordination demonstrates a more compact clustering of samples, indicative of habitat homogenization under persistently anoxic conditions. Apparent inconsistencies between microbial composition and geochemical signatures likely reflect taxonomic resolution limits and indicate finer-scale functional stratification (see Sect. 3.4).

The comparison of chemical gradients between locations B and C illustrates that the sediment permeability may exert primary control hyporheic biogeochemical functioning by regulating transport pathways, hyporheic exchange processes of SW and pore water and, therefore, the availability of EAs. Porewater geochemistry and microbial community structure respond in a coherent manner to these sediment-mediated constraints, suggesting that rather sediment permeability and OC availability control both, the chemical expression of redox processes and the microhabitat accessible to microbial communities, while the microbial composition within the sediment only indirectly determines the redox zonation.

https://doi.org/10.5194/egusphere-2026-2718
Preprint. Discussion started: 27 May 2026

3.3 Inverse modeling results as strong evidence for the effect of sediment characteristics on chemical gradients

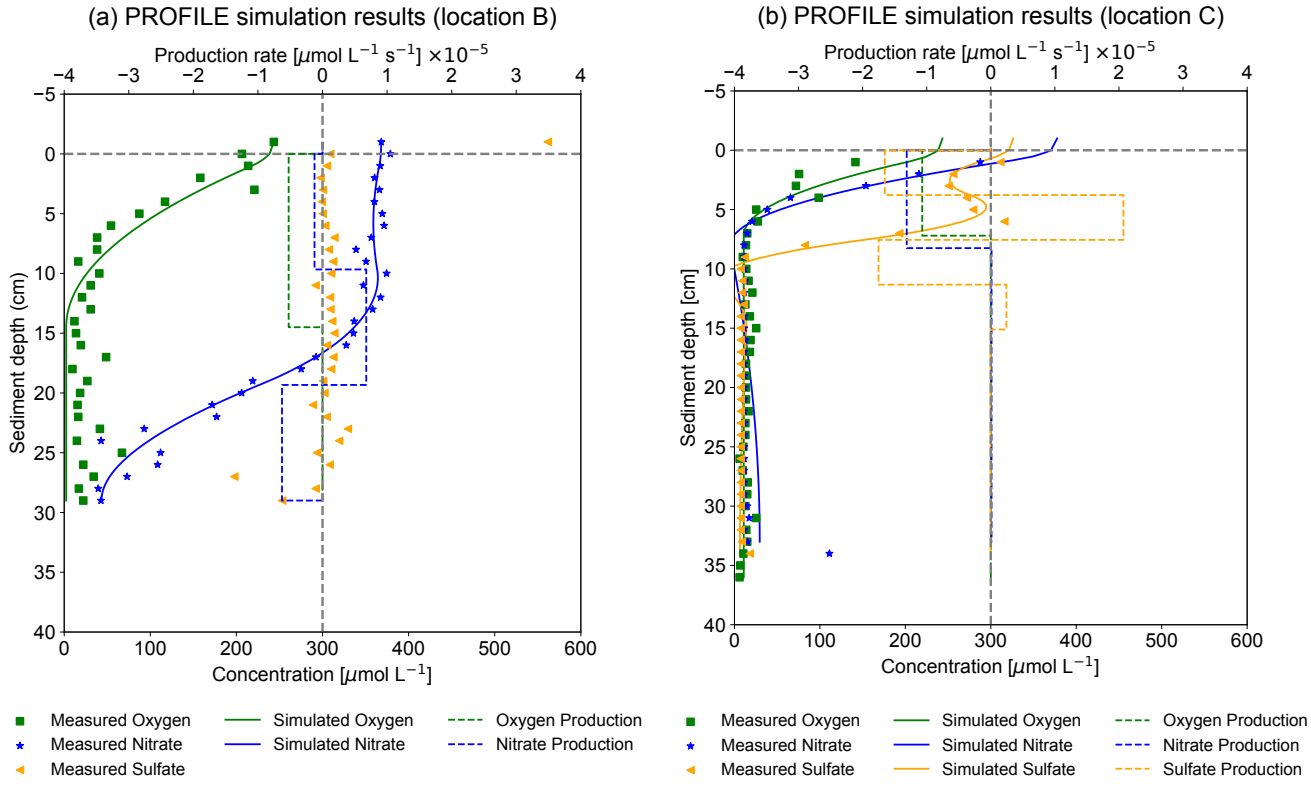

Figure 4. Depth-resolved concentration profiles and net reaction rates of oxygen, nitrate, and sulfate derived from PROFILE simulations at locations B (a) and C (b), including measured and simulated concentrations and depth-dependent zones and rates of net production and consumption.

PROFILE simulations were employed to quantify depth-resolved net consumption or production and apparent supply rates of terminal EAs. Additionally, these simulations were used to assess how sediment-controlled transport conditions influence redox zonation within the HZ at locations B and C. The modeled production-consumption terms reflect net reaction rates (μmol L^{-1} s^{-1}), incorporating the combined effects of biogeochemical reactions and transport-driven concentration gradients.

At location B, oxygen demonstrates a broad net consumption zone that extends from the sediment surface to approximately 14.5 cm, characterized by a relatively moderate and nearly uniform net consumption rate of 5.24×10^{-6} μmol L^{-1} s^{-1} (Fig. 4a). This extensive yet low-intensity oxygen consumption probably indicates efficient vertical porewater exchange within the cleaned gravel layer, facilitating deep oxygen penetration while allowing for gradual consumption rather than abrupt depletion. The nitrate reaction patterns at location B exhibit greater complexity. In the upper 0-9.7 cm, PROFILE shows net nitrate consumption at a rate of 1.24×10^{-6} μmol L^{-1} s^{-1}, which partially overlaps with the oxygen consumption zone. However, this rate is an order of magnitude lower than the concurrent oxygen consumption rate, implying that nitrate reduction in this interval is absent or quite low. Such low apparent consumption could reflect the existence of anaerobic

https://doi.org/10.5194/egusphere-2026-2718
Preprint. Discussion started: 27 May 2026

micro-niches within an otherwise oxic sediment matrix (Storey et al., 1999) or minor concentration fluctuations driven by hydraulic mixing rather than sustained biogeochemical nitrate reduction. Also, at intermediate depths (9.7-19.3 cm), PROFILE reveals a net nitrate source of 6.77×10^{-6} µmol L^{-1} s^{-1}, followed by a renewed net consumption below 19.3 cm at 6.28×10^{-6} µmol L^{-1} s^{-1}. This intermediate source term is best explained by a poor in situ nitrate reduction zone in micro-pores. Below approximately 19.3 cm, oxygen is largely depleted, and nitrate becomes the predominant terminal EA, indicating the establishment of a denitrification zone, which in accordance with the classical redox sequence. Furthermore, the similarity in nitrate consumption rates below 19.3 cm and the apparent source term above suggests that nitrate distributions are influenced by a balance between transport-limited resupply and reaction-driven removal.

Oxygen consumption at location C is restricted to the shallow sediment, occurring within the upper 0-7.2 cm and achieving net consumption rates of 1.07×10^{-5} µmol L^{-1} s^{-1} (Fig. 4b), approximately double those recorded at location B. Nitrate exhibits a similar reaction pattern, with nearly complete net consumption occurring within the upper 0-8.2 cm at a rate of 1.31×10^{-5} µmol L^{-1} s^{-1}. The significant vertical overlap between oxygen and nitrate reduction suggests that nitrate reduction can occur concurrently with oxygen consumption in shallow sediment layers. This observation aligns with the formation of anaerobic micro-zones, which are influenced by fine-grained sediment infilling and heterogeneous pore-space architecture. Beneath these shallow reaction zones, the net reaction rates for both EAs rapidly approach zero, suggesting that the supply of EAs to deeper sediment layers is significantly transport-limited. In contrast to location B, the redox zonation at location C exhibits pronounced vertical compression along with substantially higher reaction intensities. This pattern, consistent for both oxygen and nitrate, reflects transport limitation caused by fine-sediment infilling, which reduces hydraulic conductivity and EA supply, while enhanced OC availability provides sufficient electron donors, jointly intensifying biogeochemical reactions. Consequently, redox reactions become concentrated in a thin surface layer, leading to highly intensified but spatially compressed consumption zones.

Sulfate reduction is exclusively observed at location C, exhibiting a distinctly layered reaction structure. Net sulfate consumption occurs within specific depth intervals, most notably at 0-3.8 cm (1.65×10^{-5} µmol L^{-1} s^{-1}) and 7.6-11.3 cm (1.75×10^{-5} µmol L^{-1} s^{-1}), indicating active sulfate reduction under transport-limited, anaerobic conditions. The presence of sulfate consumption in the shallow 0-3.8 cm interval, despite the concurrent availability of oxygen, suggests the formation of anaerobic microzones within the sediment matrix. These sulfate reduction zones are interspersed with apparent sulfate source terms, particularly at 3.8-7.6 cm (2.07×10^{-5} µmol L^{-1} s^{-1}) and 11.3-15.1 cm (2.44×10^{-6} µmol L^{-1} s^{-1}). Such positive reaction terms are most plausibly attributed to the upward diffusion and partial reoxidation of reduced sulfur species (HS^-/H_2S) generated in deeper sulfate-reducing layers, along with vertical or lateral replenishment by sulfate-enriched porewaters. Importantly, these source terms do not signify a reversal of the net redox pathway but rather reflect the superposition of transport and reoxidation processes within a vertically compressed reaction framework. Below approximately 15.1 cm, the reaction rates of sulfate decrease sharply to 2.42×10^{-8} µmol L^{-1} s^{-1}, suggesting that sulfate has been predominantly depleted

https://doi.org/10.5194/egusphere-2026-2718
Preprint. Discussion started: 27 May 2026

or rendered kinetically inaccessible. This depth signifies the shift to a consistently anaerobic environment where sulfate reduction ceases to function as an active terminal electron-accepting process.

PROFILE simulations reveal a fundamental contrast between the two sites. Location B is characterized by relatively broad but low-intensity reaction zones, which align with an advective-dispersive transport regime that facilitates efficient porewater exchange and reduces local reaction rates. In contrast, location C displays narrowly confined yet high-intensity reaction zones, indicative of diffusion-dominated transport conditions resulting from fine-sediment infilling and a quite strong hydraulic isolation from SW, while elevated OC availability further sustains reaction intensity. These quantitative differences support the redox zonation inferred from porewater concentration profiles and demonstrate that sediment characteristics exert primary control not only on the depth distribution but also on the intensity of electron-acceptor-consuming processes.

3.4 Distribution of microbial communities closely linked to methanogenesis, methane oxidation and bacterial sulfate reduction

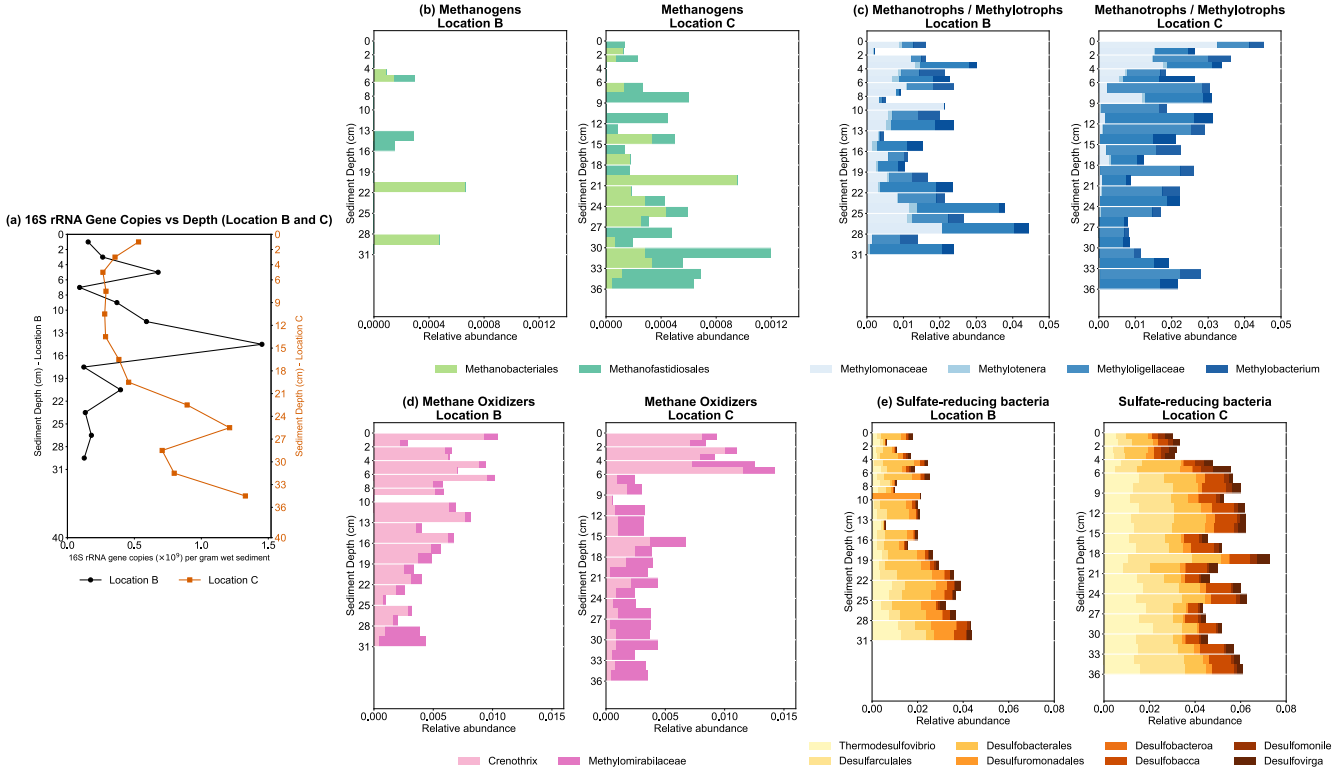

Figure 5. Depth-resolved distribution of microbial communities at locations B and C based on qPCR analyses and 16S rRNA gene sequencing. The figure shows total 16S rRNA gene copy numbers (a) and the relative abundance of major microbial functional groups, including methanogens (b), methanotrophs (c), methane oxidizers (d) and sulfate-reducing bacteria (e), as a function of sediment depth.

https://doi.org/10.5194/egusphere-2026-2718
Preprint. Discussion started: 27 May 2026

Quantification of 16S rRNA gene copy numbers reveal distinct depth-dependent variations in microbial standing stock at both locations B and C (Fig. 5a). The 16S rRNA gene copy numbers are reported as means of duplicate samples, while relative abundances are shown for both replicates. The magnitudes of copy numbers are comparable between the two locations, suggesting that both environments support microbial communities of similar overall size. Consequently, the marked differences in biogeochemical behavior observed between locations B and C are likely driven by variations in the relative abundance, vertical distribution, and organization of specific functional microbial groups.

Methanogenic archaea display markedly different vertical distribution patterns at locations B and C, which aligns with the distinct methane regimes inferred from porewater chemistry (Fig. 5b). At location B, the abundance of methanogen-associated genes remains low throughout the entire sampled interval, exhibiting no systematic increase with depth. This distribution correlates with the absence of methane accumulation, suggesting that methanogenesis does not serve as a significant terminal carbon transformation process. In contrast, at location C, methanogens demonstrate a systematic increase in abundance below approximately 24 cm, which coincides with notable methane accumulation and significantly depleted $\delta^{13}C\text{-}CH_4$ values. The methanogenic community is predominantly composed of Methanobacteriales and Methanofastidiosales, both of which are linked to non-acetoclastic methanogenic pathways (Feehan et al., 2023; Vanwonterghem et al., 2016). Methanobacteriales are typically associated with hydrogenotrophic methanogenesis through CO_2 reduction, while Methanofastidiosales are capable of methylotrophic methanogenesis utilizing methylated substrates such as methanol. The observed $\delta^{13}C\text{-}CH_4$ values, ranging from approximately -60 ‰ to -80 ‰, fall within the characteristic isotopic range of non-acetoclastic methanogenesis, thereby excluding acetoclastic methanogenesis as a dominant pathway.

Aerobic methane-oxidizing bacteria are present throughout the sediment columns at both locations B and C, exhibiting depth-dependent variations in relative abundance that are only partially associated with porewater redox conditions (Fig. 5c). These communities are primarily composed of lineages affiliated with Methylomonaceae and Methyloligellaceae, which are recognized as canonical aerobic methanotrophs that utilize O_2 as the terminal EA for methane oxidation. At location B, aerobic methanotrophs are more abundant in the shallow sediment (0-9 cm), where oxic to suboxic conditions prevail and dissolved oxygen remains detectable but is rapidly consumed. Although methane does not accumulate at this site, the presence of these taxa suggests a latent potential for methane oxidation under conditions of low or episodic methane flux, rather than sustained, high-rate oxidation. At location C, aerobic methanotrophs attain maximum relative abundances in the surface sediment (0-7 cm), which coincides with significant methane depletion and marked enrichment in $\delta^{13}C\text{-}CH_4$. This spatial relationship provides compelling microbiological evidence for active MOx in the shallow sediment, aligning with high EA availability and steep methane gradients. Importantly, aerobic methanotrophs remain detectable at substantial relative abundances in deeper hypoxic to anoxic sediment at both locations. This persistence may indicate that 16S rRNA gene-based relative abundances reflect more microbial presence than in situ activity. Their presence at depth likely signifies dormant or inactive cells, hydrological redistribution, or legacy community signals. Therefore, it should not be construed as evidence of active MOx without independent geochemical or isotopic corroboration.

https://doi.org/10.5194/egusphere-2026-2718
Preprint. Discussion started: 27 May 2026

Anaerobic and facultative methane-oxidizing microorganisms display distinct site-specific distribution patterns that closely align with sediment redox structure and the availability of EAs (Fig. 5d). This assemblage is primarily dominated by two functionally distinct groups: Crenothrix, a facultative methane oxidizer that can alternate between aerobic and nitrate-dependent methane oxidation (Oswald et al., 2017), and Candidatus Methylomirabilis, which carries out NO_2^--DAMO (Ettwig et al., 2010). Crenothrix is preferentially associated with sediment intervals characterized by oxygen consumption and nitrate reduction (Umezawa et al., 2025). At location B, it exhibits relatively high abundances throughout much of the sediment column, despite the lack of methane accumulation. This pattern suggests that, although methane supply is insufficient to sustain measurable net oxidation, the prevailing redox conditions, specifically, the availability of oxygen and nitrate, create a physicochemical environment that supports microbial communities with methane-oxidizing potential. At location C, Crenothrix is most abundant in the shallow 0-7 cm zone, where oxygen and nitrate are concurrently reduced, reflecting its metabolic versatility under fluctuating EA conditions. Its sharp decline below the nitrate reduction zone indicates that Crenothrix is not favored in environments where neither oxygen nor nitrate is present. In contrast, Candidatus Methylomirabilis exhibits a distribution that aligns with nitrite-dependent methane oxidation (Ettwig et al., 2010). At location B, its relative abundance remains low throughout the profile, which corresponds with the lack of nitrite accumulation and conditions conducive to N-DAMO. At location C, although it is not predominant in the shallow nitrate reduction zone (0-6 cm), its abundance progressively increases toward the methane oxidation layer. This depth-dependent enrichment implies a growing significance of nitrite-dependent methane oxidation near the lower boundary of methane attenuation, even in the absence of detectable nitrite accumulation. Rather than suggesting nitrite limitation, this pattern likely indicates rapid nitrite turnover, which results from the close coupling between nitrate reduction and methane oxidation. At location C, the coexistence of oxygen and nitrate reduction within the shallow sediment (0-7 cm) complicates the identification of a single dominant EA for methane oxidation based solely on hydrochemical profiles. This uncertainty is reflected in the microbial data, which reveal the presence of aerobic methanotrophs, facultative methane oxidizers (Crenothrix), and strictly anaerobic N-DAMO organisms (Candidatus Methylomirabilis). Collectively, these findings suggest that multiple pathways for methane oxidation may operate simultaneously within a narrow sediment interval, influenced by fine-scale redox heterogeneity rather than a distinct, isolated reaction zone.

Sulfate-reducing bacteria (SRB) are found at both locations B and C, yet they exhibit contrasting depth distributions that align with variations in sulfate dynamics (Fig. 5e). At location B, sulfate reducers maintain low and relatively uniform relative abundances throughout the sediment profile, which corresponds to constant sulfate concentrations and the lack of bacterial sulfate reduction. This pattern suggests that sulfate reduction is not a significant terminal process at this site. In contrast, at location C, sulfate reducers show a localized increase in relative abundance exactly there, where sulfate concentrations begin to decline. Although we have not measured H2S directly in the field because of limited sampling amounts, the onset of bacterial sulfate reduction under transport-limited, anaerobic conditions can be assumed. Notably, despite the concurrent presence of sulfate reduction in the presence of methane at location C, there is no microbial evidence

https://doi.org/10.5194/egusphere-2026-2718
Preprint. Discussion started: 27 May 2026

supporting sulfate-dependent anaerobic methane oxidation (S-DAMO). Canonical ANME lineages (ANME-1, ANME-2a/b/c, or ANME-3), which are essential for mediating S-DAMO in syntrophic association with SRB, are not detected at either site. Therefore, sulfate reduction is probably more accurately interpreted as being coupled to heterotrophic organic matter oxidation rather than to AOM at both locations.

3.5 1D reactive transport modeling results indicate domination of anaerobic methane oxidation

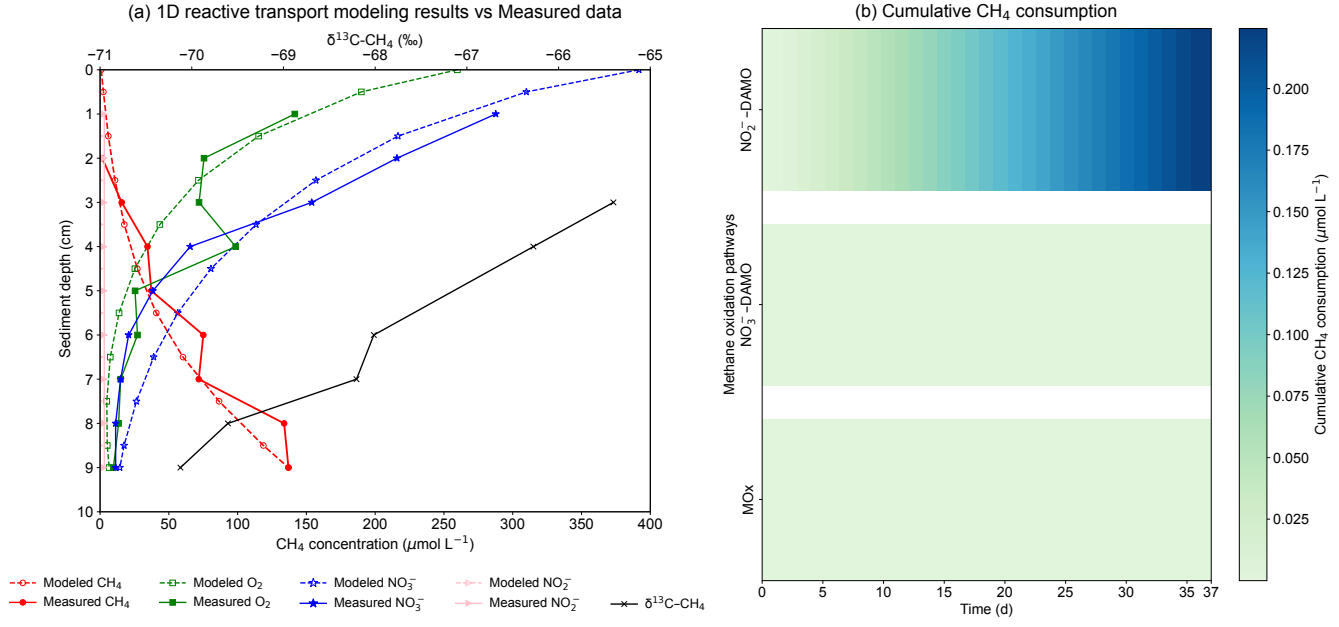

Figure 6. PHREEQC-based simulation of methane dynamics and associated redox processes in hyporheic sediments. (a) Comparison of measured and PHREEQC-simulated depth profiles of EAs (O_2, NO_3^- , NO_2^-), CH_4 and $\delta^{13}C$-CH_4. (b) Cumulative methane consumption attributed to different oxidation pathways derived from PHREEQC simulations, including NO_2^--DAMO, NO_3^--DAMO and MOx. Values represent depth-integrated methane consumption over the modeled sediment interval.

At location C, within the shallow sediment (0-9 cm), porewater CH_4 concentrations and $\delta^{13}C$-CH_4 values indicate a distinct zone of methane oxidation. Concurrently, O_2 and NO_3^- concentrations decline within the same interval, suggesting that the depletion zones for both potential terminal EAs overlap. Consequently, the solute profiles and stable isotope profiles alone do not clarify whether methane oxidation is primarily driven by aerobic processes (using O_2 as the EA) or by nitrate/nitrite-linked anaerobic pathways (NO_3^-- and NO_2^--DAMO).

To clarify this, we employed a one-dimensional reactive transport model for the 0-9 cm interval, aiming to quantify pathway partitioning under conditions of coupled transport (including advection, dispersion, and diffusion) and reation (monod kinetics).

The model not only simulates the concentration dynamics of CH_4, O_2, NO_3^- and NO_2^-, but also provides depth- and time-resolved CH_4 consumption rates for each Monod pathway, including MOx, NO_3^--DAMO, and NO_2^--DAMO (Fig S5, 6 and

https://doi.org/10.5194/egusphere-2026-2718
Preprint. Discussion started: 27 May 2026

7). These pathway-specific methane oxidation rates serve as explicit reaction terms (R_i) that contribute to the modeled concentration changes. The $\delta^{13}C$-CH_4 profile is presented alongside the concentration data to demonstrate that the modeled domain aligns with the isotopically constrained methane oxidation zone (Fig. 6a). However, stabe isotope ratios of methane are neither simulated nor utilized for calibration.

The pathway-specific methane consumption rates simulated by the model were integrated over the full simulation period (37 days) to quantify the cumulative contribution of each oxidation pathway (Fig. 6b). The resulting cumulative methane consumption fluxes clearly demonstrate a strong dominance of NO_2^--DAMO within the methane oxidation zone. Over the simulation period, NO_2^--DAMO accounts for a cumulative methane consumption of 2.24×10^{-1} µmol L^{-1}, whereas MOx and NO_3^--DAMO contribute only 3.25×10^{-4} µmol L^{-1} and 8.27×10^{-4} µmol L^{-1}, respectively. The total cumulative methane consumption amounts to 2.26×10^{-1} µmol L^{-1}, indicating that NO_2^--DAMO alone contributes more than 99 % of the total simulated methane oxidation, while the combined contribution of MOx and NO_3^--DAMO remains below 1 %.

Model results suggest that methane oxidation within the investigated sediment interval is dominated by anaerobic processes, consistent with observations from stratified lake environments (Peña Sanchez et al., 2022), among which NO_2^--DAMO emerges as the primary pathway. This outcome together with the microbial community results (Fig. 5) provides a mechanistic explanation for the apparent discrepancy between active nitrate reduction and nitrite concentrations below the DL in the porewater profiles. Although simulated aqueous NO_2^- concentrations remain below to DL, the modeled reaction network implies that nitrite can act as a highly dynamic intermediate, being transiently produced during denitrification and partially rapidly consumed as an EA for methane oxidation, consistent with observations from lake sediments (Deutzmann et al., 2014). This interpretation does not rely on the detection of nitrite in porewater, but rather on the modelling results which suggest nitrite as a short-lived intermediate with a high internal turnover rate. Within this scenario, nitrate does not primarily serve as a direct terminal EA for methane oxidation. Instead, nitrate reduction sustains a continuous internal supply of nitrite, which in turn fuels NO_2^--DAMO. The modeled methane consumption fluxes support this interpretation, as cumulative NO_2^--DAMO fluxes substantially exceed those associated with MOx and NO_3^--DAMO pathways, which together contribute less than one percent of the total simulated methane consumption over the modeled period.

It should be emphasized that these results represent one plausible and internally consistent scenario constrained by the available geochemical observations, microbial community data, and kinetic assumptions. While alternative pathway combinations cannot be excluded, the dominance of NO_2^--DAMO within the modeled methane oxidation budget demonstrates that this mechanism is capable of reconciling the observed concentration profiles with the inferred microbial functional potential in the methane oxidation zone.

https://doi.org/10.5194/egusphere-2026-2718
Preprint. Discussion started: 27 May 2026

4 Conclusion and outlook

Methane emissions from riverine sediments constitute a crucial yet highly uncertain component of the global carbon cycle, particularly under ongoing climate warming. Our results demonstrate that sediment characteristics act as a first-order control on methane cycling in the HZ. Among these, sediment permeability and OC availability represent the two key parameters governing biogeochemical processes. Sediment permeability determines the dominant transport regime and controls the penetration of EAs into deeper sediments, while OC availability regulates electron donor supply. Together, these parameters shape hydrochemical profiles, geochemical zonation, microbial community distribution, and biogeochemical reaction rates, and thus whether methanogenesis and methane oxidation can occur. Additionally, OC reactivity may represent a controlling factor, but this remains to be verified by future studies due to the absence of direct measurements. High-permeability sediments maintain oxic to suboxic conditions through efficient advective exchange, which, in combination with limited OC content, suppresses methanogenesis. In contrast, low-permeability sediments promote diffusion-dominated transport and, together with enhanced OC availability, facilitate the development of anaerobic conditions, methanogenesis, and methane oxidation. By integrating porewater chemistry, microbial community analysis, and inverse reactive transport modeling, this study further demonstrates that AOM represents the dominant methane sink under transport-limited conditions, with nitrate- and nitrite-coupled pathways as the most plausible mechanisms. These findings highlight that sediment-controlled transport-reaction coupling ultimately regulates biological methane production and oxidation, thus controls the potential for methane emissions from riverine sediments. Based on these findings, a mechanistic understanding of how sediment characteristics regulate methane production and oxidation provides a foundation for scaling process-level insights to larger spatial and temporal domains. Integrating such process-based knowledge into predictive frameworks will be essential for reducing uncertainties in methane emissions from natural aquatic systems. However, significant uncertainties remain regarding the quantitative implications for methane budgets, particularly in terms of how contrasting sedimentary regimes differ in their methane oxidation potential and how microbial community composition influences effective methane removal. Addressing these questions will require integrated experimental and modeling approaches that better constrain process rates and pathway-specific contributions. Such efforts are critical for improving predictions of methane emissions and assessing their role in the context of ongoing climate change.

Code and data availability

The hydrological data used in this study are publicly available from the Bavarian State Office for the Environment through the Gewässerkundlicher Dienst Bayern at https://www.gkd.bayern.de/en/ (Bavarian State Office for the Environment, 2025). Selected data supporting the findings of this study are provided in the Supplement. All data and code will be made available upon from the corresponding author upon request.

https://doi.org/10.5194/egusphere-2026-2718
Preprint. Discussion started: 27 May 2026

The simulations in this study were performed using the software packages PROFILE (Berg et al., 1998), which is publicly accessible at https://berg.evsc.virginia.edu/modeling-and-profile/ and PHREEQC (Parkhurst and Appelo, 2013), available at https://www.usgs.gov/software/phreeqc-version-3.

Author contributions

Conceptualization was performed by FE. Methodology was developed by YW, AW, and FE. Investigation was performed by YW, MB, AW, and WO. Data curation, software development, and visualization were conducted by YW. Formal analysis was carried out by YW and FE. Resources were provided by JG, WO, and FE. Project administration and supervision were led by FE. Funding acquisition was secured by FE. Writing of the original draft was primarily carried out by YW and FE, and all authors contributed to reviewing and editing the manuscript.

Competing interests

The authors declare that they have no conflict of interest.

Acknowledgements

We thank the technical team of the Chair of Aquatic Systems Biology at the Technical University of Munich (TUM), especially Nico Geveke, for their assistance during fieldwork. We also thank Rebecca Höß for her support with sediment sampling using the freeze-coring method and for conducting loss on ignition (LOI) analyses. In addition, we want to thank Jaroslava Obel for her assistance during field work and with laboratory analyses.

References

Aben, R. C. H., Barros, N., van Donk, E., Frenken, T., Hilt, S., Kazanjian, G., Lamers, L. P. M., Peeters, E. T. H. M., Roelofs, J. G. M., Senerpont Domis, L. N. de, Stephan, S., Velthuis, M., van de Waal, D. B., Wik, M., Thornton, B. F., Wilkinson, J., DelSontro, T., and Kosten, S.: Cross continental increase in methane ebullition under climate change, Nature communications, 8, 1682, https://doi.org/10.1038/s41467-017-01535-y, 2017.

Auerswald, K. and Geist, J.: Extent and Causes of Siltation in a Headwater Stream Bed: Catchment Soil Erosion is Less Important than Internal Stream Processes, Land Degrad Dev, 29, 737–748, https://doi.org/10.1002/ldr.2779, 2017.

Auerswald, K., Fischer, F. K., Winterrath, T., and Brandhuber, R.: Rain erosivity map for Germany derived from contiguous radar rain data, Hydrol. Earth Syst. Sci., 23, 1819–1832, https://doi.org/10.5194/hess-23-1819-2019, 2019.

https://doi.org/10.5194/egusphere-2026-2718
Preprint. Discussion started: 27 May 2026

Baulch, H. M., Dillon, P. J., Maranger, R., and Schiff, S. L.: Diffusive and ebullitive transport of methane and nitrous oxide from streams: Are bubble-mediated fluxes important?, J. Geophys. Res., 116, https://doi.org/10.1029/2011JG001656, 2011.

Bavarian State Office for the Environment: Gewässerkundlicher Dienst Bayern, https://www.gkd.bayern.de/en/, 2025.

Berg, P., Risgaard-Petersen, N., and Rysgaard, S.: Interpretation of measured concentration profiles in sediment pore water, Limnology & Oceanography, 43, 1500–1510, https://doi.org/10.4319/lo.1998.43.7.1500, 1998.

Buriánková, I., Brablcová, L., Mach, V., Hýblová, A., Badurová, P., Cupalová, J., áp, L., and Rulík, M.: Methanogens and methanotrophs distribution in the hyporheic sediments of a small lowland stream, fal, 181, 87–102, https://doi.org/10.1127/1863-9135/2012/0283, 2012.

Conrad, R.: The global methane cycle: recent advances in understanding the microbial processes involved, Environmental microbiology reports, 1, 285–292, https://doi.org/10.1111/j.1758-2229.2009.00038.x, 2009.

Crawford, J. T., Stanley, E. H., Spawn, S. A., Finlay, J. C., Loken, L. C., and Striegl, R. G.: Ebullitive methane emissions from oxygenated wetland streams, Global change biology, 20, 3408–3422, https://doi.org/10.1111/gcb.12614, 2014a.

Crawford, J. T., Lottig, N. R., Stanley, E. H., Walker, J. F., Hanson, P. C., Finlay, J. C., and Striegl, R. G.: CO 2 and CH 4 emissions from streams in a lake-rich landscape: Patterns, controls, and regional significance, Global Biogeochemical Cycles, 28, 197–210, https://doi.org/10.1002/2013GB004661, 2014b.

Cui, P., Li, H., Cui, L., and Su, F.: Sediment particle size distribution, source of organic matter and environmental implications in the Liao River, northeast China, CATENA, 249, 108696, https://doi.org/10.1016/j.catena.2024.108696, 2025.

Deutzmann, J. S., Stief, P., Brandes, J., and Schink, B.: Anaerobic methane oxidation coupled to denitrification is the dominant methane sink in a deep lake, Proceedings of the National Academy of Sciences of the United States of America, 111, 18273–18278, https://doi.org/10.1073/pnas.1411617111, 2014.

Edgar, R. C.: UPARSE: highly accurate OTU sequences from microbial amplicon reads, Nature methods, 10, 996–998, https://doi.org/10.1038/nmeth.2604, 2013.

Einsiedl, F., Wunderlich, A., Sebilo, M., Coskun, Ö. K., Orsi, W. D., and Mayer, B.: Biogeochemical evidence of anaerobic methane oxidation and anaerobic ammonium oxidation in a stratified lake using stable isotopes, Biogeosciences, 17, 5149–5161, https://doi.org/10.5194/bg-17-5149-2020, 2020.

EPA: Technical Guidance for the Natural Attenuation Indicators: Methane, Ethane, and Ethene, U.S. Environmental Protection Agency, 2001.

Ettwig, K. F., Butler, M. K., Le Paslier, D., Pelletier, E., Mangenot, S., Kuypers, M. M. M., Schreiber, F., Dutilh, B. E., Zedelius, J., Beer, D. de, Gloerich, J., Wessels, H. J. C. T., van Alen, T., Luesken, F., Wu, M. L., van de Pas-Schoonen, K. T., Op den Camp, H. J. M., Janssen-Megens, E. M., Francoijs, K.-J., Stunnenberg, H., Weissenbach, J., Jetten, M. S. M., and Strous, M.: Nitrite-driven anaerobic methane oxidation by oxygenic bacteria, Nature, 464, 543–548, https://doi.org/10.1038/nature08883, 2010.

https://doi.org/10.5194/egusphere-2026-2718
Preprint. Discussion started: 27 May 2026

Feehan, B., Ran, Q., Dorman, V., Rumback, K., Pogranichniy, S., Ward, K., Goodband, R., Niederwerder, M. C., and Lee, S. T. M.: Novel complete methanogenic pathways in longitudinal genomic study of monogastric age-associated archaea, Animal microbiome, 5, 35, https://doi.org/10.1186/s42523-023-00256-6, 2023.

Fischer, H., Kloep, F., Wilzcek, S., and Pusch, M. T.: A River's Liver – Microbial Processes within the Hyporheic Zone of a Large Lowland River, Biogeochemistry, 76, 349–371, https://doi.org/10.1007/s10533-005-6896-y, 2005.

Geist, J. and Auerswald, K.: Physicochemical stream bed characteristics and recruitment of the freshwater pearl mussel (Margaritifera margaritifera), Freshwater Biology, 52, 2299–2316, https://doi.org/10.1111/j.1365-2427.2007.01812.x, 2007.

Geist, J., Hoess, R., Rytterstam, J., and Söderberg, H.: Substratum Raking Can Restore Interstitial Habitat Quality in Swedish Freshwater Pearl Mussel Streams, Diversity, 15, 869, https://doi.org/10.3390/d15070869, 2023.

Hassan, J., Qu, Z., Bergaust, L. L., and Bakken, L. R.: Transient Accumulation of NO2- and N2O during Denitrification Explained by Assuming Cell Diversification by Stochastic Transcription of Denitrification Genes, PLoS computational biology, 12, e1004621, https://doi.org/10.1371/journal.pcbi.1004621, 2016.

Hendricks, S. P.: Microbial Ecology of the Hyporheic Zone: A Perspective Integrating Hydrology and Biology, Journal of the North American Benthological Society, 12, 70–78, https://doi.org/10.2307/1467687, 1993.

Herzog, S. P., Ward, A. S., Wondzell, S. M., Serchan, S. P., González-Pinzón, R., and Zarnetske, J. P.: Seasonality Controls Biogeochemical Shifts in Oxygen, Carbon, and Nitrogen Along a 12-m, 54 hr-Long Hyporheic Flowpath, Water Resources Research, 61, https://doi.org/10.1029/2024WR038410, 2025.

Hesslein, R. H.: An in situ sampler for close interval pore water studies1, Limnology & Oceanography, 21, 912–914, https://doi.org/10.4319/lo.1976.21.6.0912, 1976.

Hinkle, S. R., Duff, J. H., Triska, F. J., Laenen, A., Gates, E. B., Bencala, K. E., Wentz, D. A., and Silva, S. R.: Linking hyporheic flow and nitrogen cycling near the Willamette River — a large river in Oregon, USA, Journal of Hydrology, 244, 157–180, https://doi.org/10.1016/S0022-1694(01)00335-3, 2001.

Hoess, R. and Geist, J.: Spatiotemporal variation of streambed quality and fine sediment deposition in five freshwater pearl mussel streams, in relation to extreme drought, strong rain and snow melt, Limnologica, 85, 125833, https://doi.org/10.1016/j.limno.2020.125833, 2020.

IPCC: Climate Change 2021: The Physical Science Basis, Contribution of Working Group I to the Sixth Assessment Report of the Intergovernmental Panel on Climate Change [Masson-Delmotte, V., P. Zhai, A. Pirani, S.L. Connors, C. Péan, S. Berger, N. Caud, Y. Chen, L. Goldfarb, M.I. Gomis, M. Huang, K. Leitzell, E. Lonnoy, J.B.R. Matthews, T.K. Maycock, T. Waterfield, O. Yelekçi, R. Yu, and B. Zhou (eds.)]. Cambridge University Press, Cambridge, United Kingdom and New York, NY, USA, 2391 pp., 2021.

Jiang, M., Ye, C., Jiang, H., Gong, Y., and Zhang, Q.: Ecological Variability and Controls on Denitrifying Anaerobic Methane Oxidation, Global Biogeochemical Cycles, 40, https://doi.org/10.1029/2025GB008766, 2026.

https://doi.org/10.5194/egusphere-2026-2718
Preprint. Discussion started: 27 May 2026

Jørgensen, B. B., Egger, M., and Canfield, D. E.: Sulfate distribution and sulfate reduction in global marine sediments, Geochimica et Cosmochimica Acta, 364, 79–88, https://doi.org/10.1016/j.gca.2023.11.015, 2024.

Kampbell, D. H. and Vandegrift, S. A.: Analysis of dissolved methane, ethane, and ethylene in ground water by a standard gas chromatographic technique, Journal of chromatographic science, 36, 253–256, https://doi.org/10.1093/chromsci/36.5.253, 1998.

Liu, L., Yang, Z. J., Delwiche, K., Long, L. H., Liu, J., Liu, D. F., Wang, C. F., Bodmer, P., and Lorke, A.: Spatial and temporal variability of methane emissions from cascading reservoirs in the Upper Mekong River, Water research, 186, 116319, https://doi.org/10.1016/j.watres.2020.116319, 2020.

Liu, Y., Yao, T., Gleixner, G., Claus, P., and Conrad, R.: Methanogenic pathways, 13 C isotope fractionation, and archaeal community composition in lake sediments and wetland soils on the Tibetan Plateau, JGR Biogeosciences, 118, 650–664, https://doi.org/10.1002/jgrg.20055, 2013.

Ma, S., Jiang, L., Wilson, R. M., Chanton, J. P., Bridgham, S., Niu, S., Iversen, C. M., Malhotra, A., Jiang, J., Lu, X., Huang, Y., Keller, J., Xu, X., Ricciuto, D. M., Hanson, P. J., and Luo, Y.: Evaluating alternative ebullition models for predicting peatland methane emission and its pathways via data–model fusion, Biogeosciences, 19, 2245–2262, https://doi.org/10.5194/bg-19-2245-2022, 2022.

McMahon, P. B. and Böhlke, J. K.: Denitrification and mixing in a stream—aquifer system: effects on nitrate loading to surface water, Journal of Hydrology, 186, 105–128, https://doi.org/10.1016/S0022-1694(96)03037-5, 1996.

Michaelis, T., Kaplar, F., Baumann, T., Wunderlich, A., and Einsiedl, F.: High methane ebullition throughout one year in a regulated central European stream, Scientific reports, 14, 5359, https://doi.org/10.1038/s41598-024-54760-z, 2024.

Michaelis, T., Wunderlich, A., Coskun, Ö. K., Orsi, W., Baumann, T., and Einsiedl, F.: High-resolution vertical biogeochemical profiles in the hyporheic zone reveal insights into microbial methane cycling, Biogeosciences, 19, 4551–4569, https://doi.org/10.5194/bg-19-4551-2022, 2022.

Monterroso, H., Widdowson, M. A., Lotts, W. S., Strom, K. B., and Hester, E. T.: Effects of boundary hydraulics, dissolved oxygen, and dissolved organic carbon on growth and death dynamics of aerobic microbes in riverbed dune-induced hyporheic zones, The Science of the total environment, 906, 167401, https://doi.org/10.1016/j.scitotenv.2023.167401, 2024.

Müller, M., Pander, J., and Geist, J.: The ecological value of stream restoration measures: An evaluation on ecosystem and target species scales, Ecological Engineering, 62, 129–139, https://doi.org/10.1016/j.ecoleng.2013.10.030, 2014.

Oswald, K., Graf, J. S., Littmann, S., Tienken, D., Brand, A., Wehrli, B., Albertsen, M., Daims, H., Wagner, M., Kuypers, M. M., Schubert, C. J., and Milucka, J.: Crenothrix are major methane consumers in stratified lakes, The ISME journal, 11, 2124–2140, https://doi.org/10.1038/ismej.2017.77, 2017.

Pander, J., Müller, M., and Geist, J.: A Comparison of Four Stream Substratum Restoration Techniques Concerning Interstitial Conditions and Downstream Effects, River Res. Applic., 31, 239–255, https://doi.org/10.1002/rra.2732, 2015.

https://doi.org/10.5194/egusphere-2026-2718
Preprint. Discussion started: 27 May 2026

Parkhurst, D. L. and Appelo, C. A. J.: Description of input and examples for PHREEQC version 3—A computer program for speciation, batch-reaction, one-dimensional transport, and inverse geochemical calculations, 497 pp., available at: http://pubs.usgs.gov/tm/06/a43, 2013.

Peña Sanchez, G. A., Mayer, B., Wunderlich, A., Rein, A., and Einsiedl, F.: Analysing seasonal variations of methane oxidation processes coupled with denitrification in a stratified lake using stable isotopes and numerical modeling, Geochimica et Cosmochimica Acta, 323, 242–257, https://doi.org/10.1016/j.gca.2022.01.022, 2022.

Penger, J., Conrad, R., and Blaser, M.: Stable carbon isotope fractionation by methylotrophic methanogenic archaea, Applied and environmental microbiology, 78, 7596–7602, https://doi.org/10.1128/AEM.01773-12, 2012.

Pichler, M., Coskun, Ö. K., Ortega-Arbulú, A.-S., Conci, N., Wörheide, G., Vargas, S., and Orsi, W. D.: A 16S rRNA gene sequencing and analysis protocol for the Illumina MiniSeq platform, MicrobiologyOpen, 7, e00611, https://doi.org/10.1002/mbo3.611, 2018.

Pulg, U., Barlaup, B. T., Sternecker, K., Trepl, L., and Unfer, G.: RESTORATION OF SPAWNING HABITATS OF BROWN TROUT (SALMO TRUTTA) IN A REGULATED CHALK STREAM, River Res. Applic., 29, 172–182, https://doi.org/10.1002/rra.1594, 2013.

Qin, X., Li, Y., Wan, Y., Fan, M., Liao, Y., Li, Y., Wang, B., and Gao, Q.: Diffusive flux of CH4 and N2O from agricultural river networks: Regression tree and importance analysis, The Science of the total environment, 717, 137244, https://doi.org/10.1016/j.scitotenv.2020.137244, 2020.

Quast, C., Pruesse, E., Yilmaz, P., Gerken, J., Schweer, T., Yarza, P., Peplies, J., and Glöckner, F. O.: The SILVA ribosomal RNA gene database project: improved data processing and web-based tools, Nucleic acids research, 41, D590-6, https://doi.org/10.1093/nar/gks1219, 2013.

Raghoebarsing, A. A., Pol, A., van de Pas-Schoonen, K. T., Smolders, A. J. P., Ettwig, K. F., Rijpstra, W. I. C., Schouten, S., Damsté, J. S. S., Op den Camp, H. J. M., Jetten, M. S. M., and Strous, M.: A microbial consortium couples anaerobic methane oxidation to denitrification, Nature, 440, 918–921, https://doi.org/10.1038/nature04617, 2006.

Sawakuchi, H. O., Bastviken, D., Sawakuchi, A. O., Krusche, A. V., Ballester, M. V. R., and Richey, J. E.: Methane emissions from Amazonian Rivers and their contribution to the global methane budget, Global change biology, 20, 2829–2840, https://doi.org/10.1111/gcb.12646, 2014.

Schäfer, D., Schäfer, W., and Kinzelbach, W.: Simulation of reactive processes related to biodegradation in aquifers 2. Model application to a column study on organic carbon degradation, Journal of Contaminant Hydrology, 31, 187–209, https://doi.org/10.1016/S0169-7722(97)00061-2, 1998.

Schubert, C. J., Vazquez, F., Lösekann-Behrens, T., Knittel, K., Tonolla, M., and Boetius, A.: Evidence for anaerobic oxidation of methane in sediments of a freshwater system (Lago di Cadagno), FEMS microbiology ecology, 76, 26–38, https://doi.org/10.1111/j.1574-6941.2010.01036.x, 2011.

Shapiro, J.: The Core-Freezer--A New Sampler for Lake Sediments, Ecology, 39, 758, https://doi.org/10.2307/1931618, 1958.

https://doi.org/10.5194/egusphere-2026-2718
Preprint. Discussion started: 27 May 2026

Sophocleous, M.: Interactions between groundwater and surface water: the state of the science, Hydrogeology Journal, 10, 52–67, https://doi.org/10.1007/s10040-001-0170-8, 2002.

Storey, R. G., Fulthorpe, R. R., and Williams, D. D.: Perspectives and predictions on the microbial ecology of the hyporheic zone, Freshwater Biology, 41, 119–130, https://doi.org/10.1046/j.1365-2427.1999.00377.x, 1999.

Striegl, R. G., Dornblaser, M. M., McDonald, C. P., Rover, J. A., and Stets, E. G.: Carbon dioxide and methane emissions from the Yukon River system, Global Biogeochemical Cycles, 26, https://doi.org/10.1029/2012GB004306, 2012.

Taylor, S. W. and Jaffé, P. R.: Biofilm growth and the related changes in the physical properties of a porous medium: 1. Experimental investigation, Water Resources Research, 26, 2153–2159, https://doi.org/10.1029/WR026i009p02153, 1990.

Teasdale, P.: Pore water sampling with sediment peepers, TrAC Trends in Analytical Chemistry, 14, 250–256, https://doi.org/10.1016/0165-9936(95)91617-2, 1995.

Thottathil, S. D., Reis, P. C. J., and Prairie, Y. T.: Variability and controls of stable carbon isotopic fractionation during aerobic methane oxidation in temperate lakes, Front. Environ. Sci., 10, https://doi.org/10.3389/fenvs.2022.833688, 2022.

Umezawa, K., Tsuji, J. M., Tani, Y., Nohara, S., Amann, R., and Fukui, M.: Isolation of Crenothrix bacteria reveals the distinct ecophysiologies of filamentous methanotrophs and adaptations to redox stress, 2025.

Vanwonterghem, I., Evans, P. N., Parks, D. H., Jensen, P. D., Woodcroft, B. J., Hugenholtz, P., and Tyson, G. W.: Methylotrophic methanogenesis discovered in the archaeal phylum Verstraetearchaeota, Nature microbiology, 1, 16170, https://doi.org/10.1038/nmicrobiol.2016.170, 2016.

Vuillemin, A., Wankel, S. D., Coskun, Ö. K., Magritsch, T., Vargas, S., Estes, E. R., Spivack, A. J., Smith, D. C., Pockalny, R., Murray, R. W., D'Hondt, S., and Orsi, W. D.: Archaea dominate oxic subseafloor communities over multimillion-year time scales, Science advances, 5, eaaw4108, https://doi.org/10.1126/sciadv.aaw4108, 2019.